DISSERTATIONES PHYSICAE UNIVERSITATIS TARTUENSIS

15

LASER SPECTROSCOPY OF SOME JET–COOLED ORGANIC MOLECULES

by

ERKO JALVISTE

TARTU 1993

DISSERTATIONES PHYSICAE UNIVERSITATIS TARTUENSIS

15

LASER SPECTROSCOPY OF SOME JET–COOLED ORGANIC MOLECULES

by

ERKO JALVISTE

Thesis for the degree of Doctor of Philosophy in Physics

TARTU 1993

The study was performed at the Laboratory of Laser Technique, Institute of Physics of the Estonian Academy of Sciences, Tartu, Estonia.

Supervisor: A. Treshchalov, Cand. Sci.

Official opponents: S. Alimpiev , Dr. Sci.
I. Sildos , Cand. Sci.
J. Subbi , Cand. Sci.

The thesis will be defended on February 2, 1994 at 3 p.m. in the Council Hall of Tartu University, Ülikooli 18, EE2400 Tartu, Estonia.

Secretary of the Council: A. Lushchik, Dr. Sci

Erko Jalviste was born in 1962 in Tartu. In 1984 he graduated from Tartu University with the specialization in solid state physics. Since 1984 he has been working at the Laboratory of Laser Technique of the Institute of Physics, whereby since 1986 as junior research associate.

The author's permanent address:
Institute of Physics of Estonian Acad. Sci.,
Riia 142, EE2400, Tartu, Estonia.

TÜ 93. 5,4. 5,5. 200. T. 509.

© Erko Jalviste, 1994

CONTENTS

1 General introduction 5
1.1 Supersonic jet 6
1.2 Laser-induced fluorescence spectroscopy 7
1.3 Experimental set-up 9
1.4 Preview of the present work 11
References 12

2 The effect of saturation on the rotational band contours of jet-cooled quinizarin 13
2.1 Introduction 13
2.2 Experimental 14
2.3 Rotational band contours 15
2.4 The saturation curves of the 0-0 band 19
2.5 Time-dependent and laser mode-structure effects 22
2.6 Transition strength of the 0-0 band 27
References 29

3 Saturation of the fluorescence anisotropy of the quinizarin jet 31
3.1 Introduction 31
3.2 Experimental 32
3.3 The observed effects 33
3.4 Model calculations 34
3.5 Interpretation of the results 38
References 41

4 $S_1 \leftrightarrow S_0$ spectra of jet-cooled benzimidazole and benzotriazole 42
4.1 Introduction 43
4.2 Experimental 45
4.3 Benzimidazole 47
4.3.1 Excitation and 0-0 band fluoresence spectra 47
4.3.2 Fluorescence from vibronic levels of S_1 52
4.3.3 Franck-Condon analysis of the breathing mode 57

4.4 Benzotriazole 58
4.4.1 Excitation spectrum 58
4.4.2 Vibrational analysis of S_1 origin fluorescence 59
4.5 Conclusions about the excited electronic states 67
References 69

5 Supercritical CO_2 as a solvent for sample introduction into a supersonic jet for LIF spectroscopy 71
5.1 Introduction 71
5.2 Experimental 73
5.3 Results and discussion 74
References 79

Main results 82
Põhitulemused 84
Acknowledgements 86
Conferences 86
Publications 87

Chapter 1

GENERAL INTRODUCTION

A number of methods are available to gain insight in the properties of molecules by spectroscopy of their electronic states. Molecules can be studied in the vapour phase, in solution, in their own or in the host crystal or in a noble gas matrix. However, in the condensed phase and in solution the effects of the surrounding have to be considered together with the properties of a bare molecule. If one is interested in the spectroscopic behaviour of the free, isolated molecule, information can be obtained only in the vapour phase. The vapour-phase absorption spectra of intermediate and large-size organic molecules, however, exhibit rotational broadening and vibrational sequence congestion, produced by an overwhelming number of the transitions originating from thermally populated rotational and vibrational levels. This puts a constraint on the spectroscopic information that can be extracted from such a "hot" vapour spectra.

The use of a supersonic expansion allows the preparation of internally cold, isolated, gas-phase molecules and thereby retains the advantages of the solid state or matrix isolation spectroscopy at cryogenic temperatures without the disadvantage of intermolecular perturbations.

Nowadays the molecular spectroscopy using the supersonic jet together with laser excitation has undergone a very fast development. New experimental techniques have been introduced and a vast amount of refined spectroscopic information has been obtained. A review on this topic, covering a period up to 1979, has been published in Ref. [1]. Later developments (up to 1987) are reflected in the review [2]. Below only the basic principles of jet cooling and laser-induced fluorescence (LIF) spectroscopy of isolated large organic molecules on the ground of review [1], necessary for understanding the rest of this thesis, are presented.

1.1 Supersonic jet

A free supersonic jet is formed on expanding the mixture of the sample vapour and the carrier gas through a small orifice (diameter 0.1-1 mm) or nozzle into vacuum. Physically it means that the thermal energy (enthalpy) of the gas is converted into the kinetic energy of the directed flow, which results in a very low translational temperature (characterizing the distribution of random velocity component) in the jet. Commonly He or Ar are used as a carrier gas because atomic gases do not have vibrational degrees of freedom which restrict cooling. He as a better coolant is mostly used in case of a pulsed jet (its opening is synchronized with the repetition rate of the pulsed laser) but cheaper Ar is used in case of a continuous jet. The optimum stagnation pressure (pressure of the gas mixture before expansion) is some atm for He and some tenth of atm for Ar. At lower stagnation pressures cooling becomes worse (the supersonic flow turns finally into the subsonic one) and at higher pressures clustering starts (Van der Waals complexes of the molecule of interest with Ar or He atoms) or the evacuation pumps cannot maintain the vacuum because of increased flow. The other adjustable parameter stagnation temperature (temperature of the gas mixture before expansion) determines the concentration of the sample molecules in the jet. The sample compounds with lower vapour pressure require the application of higher stagnation temperature. Too low temperature lead to a weak LIF signal, but too high temperature, to an extensive self-clustering and quick exhaustion of the sample.

Rotational and vibrational degrees of freedom of the molecules introduced are cooled by the vibrational-rotational energy transfer to the cold translational bath of carrier gas atoms during the expansion into vacuum. The energy transfers by successive formation and predissociation of Van der Waals complexes (Ar with the seeded molecule) rather than simply by collisions [3]. The initial stage of expansion is nearly adiabatic. Downstream the nozzle the flow is transformed to a collisionless one without thermodynamic equilibrium between the

translational, rotational and vibrational degrees of freedom. Rotational and vibrational populations are therefore characterized by different temperatures T_{rot} and T_{vib}. Typically T_{rot} of 2-15 K and T_{vib} of 10-50 K are observed in the Ar jet. In most cases the excited state lifetime of the molecule under investigation is considerably shorter (tens of ns) than the mean time interval between collisions in the region where the jet is intersected by the laser beam. This time interval is typically longer than 1 μs as estimated by the theory from Ref. [4], thus there is no doubt in regarding the jet-cooled molecules as free ones.

Being caused by the remainder pressure of the ambient gas, the free jet is surrounded with a standing shock-wave system, as revealed by visualization of the flow [5]. The axis-symmetric shock wave (Mach barrel) ends with a planar, perpendicular to the flow axis planar shock wave called Mach disk. The temperature in the flow jumps to near its stagnation value after passing the Mach disk, therefore, the laser beam should intersect the jet before it. For our jet in typical conditions the distance from nozzle orifice to Mach disk is estimated to be of 3-6 cm using an empirical formula from Ref. [5]. The spatially dependent and non-Bolzmann population distribution, characteristic of the shock-wave structure, gives rise to the so-called hot bands in the spectra originating from vibrationally excited levels of the molecule under study. However, the lowest vibrational level is still the most populated one in the cold core of the jet.

1.2 Laser-induced fluorescence spectroscopy

Laser-induced fluorescence (LIF) spectroscopy is based on the laser excitation of a free jet and the detection of spontaneously emitted fluorescence photons. The energy absorbed from the laser beam in the jet is usually too low for a direct absorption detection but sufficient for LIF detection. There are two types of LIF spectra. In LIF excitation spectroscopy the wavelength of the exciting laser is tuned and the total undispersed fluorescence is collected, the spectrum being the

total emitted light as a function of the exciting wavelength. This spectrum is the product of the absorption spectrum and the fluorescence quantum yield. In dispersed fluorescence spectroscopy, the exciting laser is fixed at a particular absorption wavelength of the molecule and the emitted light is dispersed with a monochromator. The spectrum is the intensity of the emitted light as a function of the wavelength of the emitted light.

It should be noted that not all molecules can be investigated by the standard version of jet LIF spectroscopy: their transition strength, fluorescence quantum yield, and vapour pressure (at stagnation temperature) should be large enough in the wavelength region available to gain a noise-free LIF signal.

Excited and ground electronic state vibrational frequencies and the intensities of the vibronic bands is the direct information which can be extracted from the excitation and dispersed fluorescence spectra. The frequencies from jet spectra are in general more accurate and reliable than the ones determined from the vapour absorption spectrum because of the lack of the congestion of the bands.

Unlike vapour phase spectra, where the fluorescence comes, as a rule, from the excited state origin level after relaxation, in case of free jet there is no energy loss due to collisional relaxation. The fluorescence comes therefore from initially excited vibronic level or at least from nearly isoenergetic levels coupled to the initially excited level. These isoenergetic levels can belong to a quasicontinuum of other vibrational levels of the same electronic state (in case of intramolecular vibrational redistribution) or that of another (triplet) state (in case of intersystem crossing).

The spectral width of a pulsed dye laser radiation is usually not narrow enough to resolve individual rotational transitions of large molecules. However, it is often enough to know the shape of the rotational contour of vibronic bands to assign vibrational symmetries of respective modes. Such an assigning technique is called rotational contour analysis.

1.3 Experimental set-up

The basic configuration of the experimental set-up representing a typical LIF spectrometer is shown in Fig. 1.1. The entire set-up can formally be divided into three parts: a laser source providing for the excitation beam, the fluorescence collecting optics and signal-processing electronics, and the gas system providing for continuous work of the supersonic jet.

Laser system consists of a XeCl excimer laser, which pumps a three-stage (oscillator and two amplifiers) pulsed dye laser. If necessary, the laser beam can be frequency doubled by a KDP crystal, which is angle-tuned by an autotracer during the scans. A microprocessor-based dye-laser controller ensures a simultaneous scanning of the grating and the intracavity etalon for high-resolution scans and generates calibration marks for the wavelength scale of the spectra. The second monochromator and a Fe/Ne hollow cathode lamp serve for the calibration of the dye laser wavelength counter.

An unfocussed laser beam entering the vacuum chamber through a Brewster-angle quartz window is collimated by 3 mm-diameter diaphragms mounted inside a pipe (an arm baffle) in order to minimize the stray light. The arm baffle for the outcoming beam has larger (8 mm) diafragms. The fluorescing region of the jet is imaged by lens systems to a photomultiplier for the excitation spectra and to the entrance slits of a monocromator followed by a photomultiplier for dispersed fluorescence spectra. The signals from the photomulipliers are procecced by a boxcar integrator, the analog output of which is recorded as a spectrum on a paper sheet.

The assembly for jet formation is presented in Fig. 1.2. Ar gas from the pressure vessel is directed through a regulator and a flowmeter to the heatable sample container mounted inside the vacuum chamber, which is continuously evacuated. The distance between the jet formation orifice and the laser beam usually set to 5 mm can be varied by adjusting the height of the entire assembly. The refilling of the sample holder with a new sample after its exhaustion can be accomplished only by opening the container.

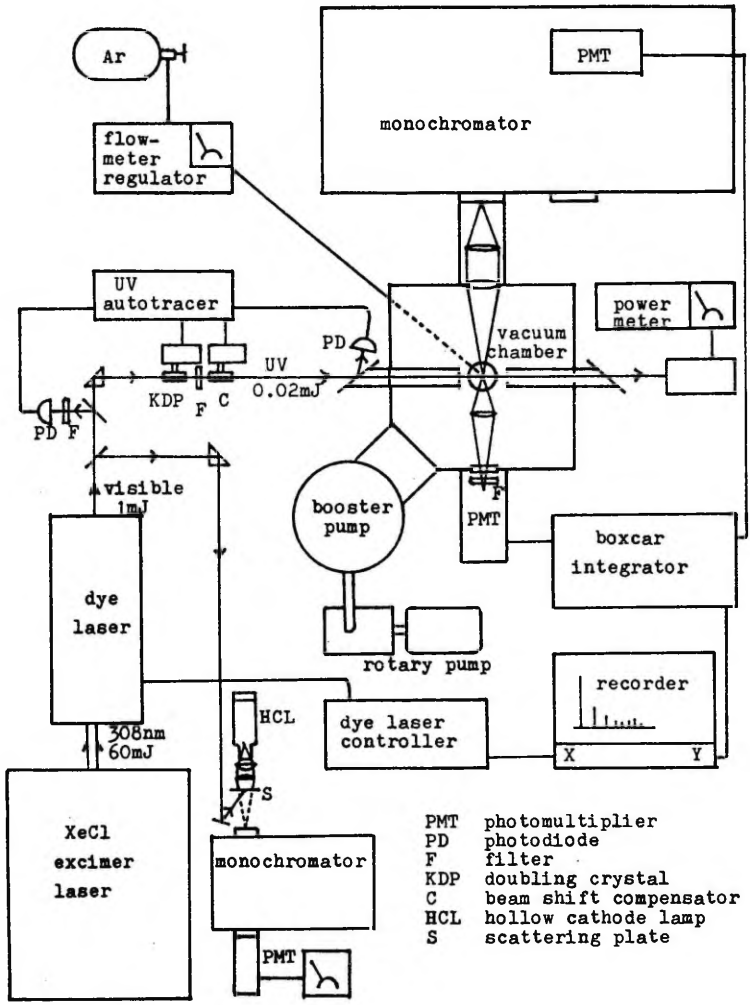

Figure 1.1: Block diagram of the experimental apparatus.

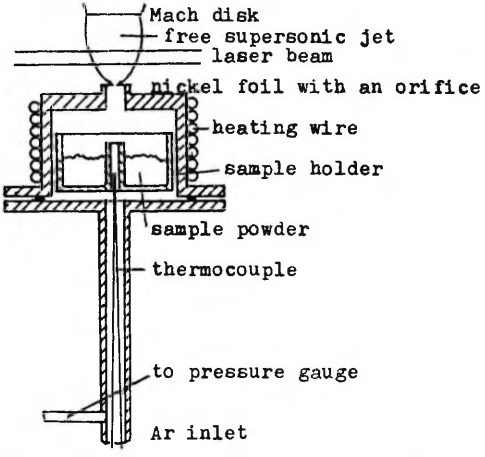

Figure 1.2: A schematic cross-section of the sample container assembly. The envelop of the shock-wave structure and the laser beam position are shown graphically . The thermocouple and the pressure gauge monitor the stagnation temperature and the stagnation pressure, respectively.

The configuration of the set-up used is accommodated to the needs of a particular experiment. Therefore a detailed description of the equipment used and the measuring technique applied is presented in the experimental sections of the following chapters.

1.4 Preview of the present work

This thesis consists of four investigations with rather different problems and aims. However, all the investigations presented are grounded on the laser-induced fluorescence (LIF) spectroscopy of free supersonic jet. Hence it can be stated that the purpose common throughout this thesis is to demonstrate many-sided possibilities of this nowadays already a standard technique.

Chapter 2 deals with the LIF saturation effect, which is important in most of the jet experiments on molecules with a large transition moment. Main attention is paid to the rotatio-

nal contour analysis and the influence of saturation on the rotational contours of quinizarin. Various effects affecting the saturation curve (fluorescence intensity as a function of the excitation intensity) are discussed.

Chapter 3, a complementary one to Chapter 2, is devoted to investigating the problems why the fluorescence from quinizarin jet is polarized and how the fluorescence polarization anisotropy of quinizarin jet is affected by saturation. The experimental results are compared with a model calculation.

In Chapter 4 benzimidazole and benzotriazole molecules are investigated. Since the jet spectra of these molecules have been measured for the first time, a detailed vibrational analysis is carried out. The interest in these molecules is motivated by the different nature of their two excited electronic states (^1L_a and ^1L_b) and by possible proton transfer effects.

Chapter 5 describes the probing of a new method for introduction low-volatile biomolecules into a supersonic jet for LIF spectroscopy. A practical outlook is the coupling of a jet-based LIF detector to a supercritical fluid chromatograph.

References

[1] D.H.Levy, Ann. Rev. Phys. Chem. 31 (1980) 197

[2] M.Ito, T.Ebata, N.Mikami, Ann. Rev. Phys. Chem. 39 (1988) 123

[3] A.Amirav, U.Even, J.Jortner, Chem. Phys. 51 (1980) 31

[4] D.M.Lubman, C.T.Rettner, R.N.Zare, J. Phys. Chem. 86 (1982) 1129

[5] R.Campargue, J. Phys. Chem. 88 (1984) 4466

Chapter 2

THE EFFECT OF SATURATION ON THE ROTATIONAL BAND CONTOURS OF JET-COOLED QUINIZARIN

2.1 Introduction

Cooling in a supersonic jet of a carrier gas is nowadays a widely used technique to obtain structured, free from thermal congestion, spectra of large organic molecules. In most of the jet experiments pulsed dye lasers, with a high peak power are used to excite molecular fluorescence. Therefore it seems quite actual to take into account the saturation effects which appear as a power-dependent distortion of excitation spectra if a molecule with a large oscillator strength is excited.

The first direct measurement of nonlinear dependence of fluorescence intensity on excitation intensity (saturation curve) was performed for K_2 vapour [1], where the transition from linear to square root dependence was interpreted as an optical saturation of a two-level system with inhomogeneous broadening. The saturation of vibronic spectra of antracene and perylene impurity molecules in cooled matrices has been studied in Refs. [2,3]; dipole moments of vibronic transitions and fluorescence lifetimes of a number of S_1 levels have been obtained by processing the saturation curves for excitation and for stimulated dumping. The saturation of vibronic excitation spectra of jet-cooled quinizarin has been examined and the dependence of the laser mode-structure on saturation intensity was estimated in Ref. [4].

Tunable narrow-bandwidth dye lasers permit to resolve the rotational contour shape of vibronic bands in the excitation spectrum of large jet-cooled organic molecules. An analysis of rotational band contours can give valuable information about the rotational temperature, relaxation rates, the transition dipole moment direction, the extent of the geometry change upon the electronic transition even if the individual rotational lines cannot be resolved. Vibrational symmetries of the modes corresponding to the observed bands can often be assigned by

their contours [5].

The present work has aimed at the measuring of the saturation curve for the 0-0 band of $S_1 \leftarrow S_0$ transition, an analysis of rotational contour shapes of vibronic bands in the $S_1 \leftarrow S_0$ excitation spectrum and an investigation of the distortion of the 0-0 band contour at high excitation intensities.

2.2 Experimental

A free continuous jet of cooled 1,4-dihydroxy-9,10-antraquinone (quinizarin) molecules was formed by expanding a mixture of quinizarin vapour and Ar carrier gas at 16 kPa into vacuum through a 0.2 mm orifice. To get sufficient vapour pressure the quinizarin powder was heated up to 140°C. The measured Ar flow rate was ≈20 $cm^3 \cdot atm/min$. The vacuum chamber was pumped by a booster pump NVBM-0.5 (700 l/s) backed by a rotary pump 2NVR-5D (5 l/s), which ensured a vacuum of 0.1 Pa.

The fluorescence of quinizarin was excited with a VL-18 pulsed dye laser (coumarin-30 dye) pumped by a ELI-5 excimer laser. The spectral width (FWHM) of VL-18 radiation, measured by calibrated interferometers, was 0.25 cm^{-1} and 0.045 cm^{-1} without and with an 5 mm (0.67 cm^{-1} FSR) intracavity etalon, respectively. Typical pulse energy, measured by an IMO-2N power-energy meter, was 0.8 mJ. Pulse-to-pulse stability was about 5% (with an etalon 0.2 mJ and 20%, respectively). The temporal shape of the laser pulse, recorded with a fast-response vacuum photoelement FEK-22, was close to a Gaussian with FWHM 4 ns. An unfocussed laser beam with the cross-section of about 3 mm^2 was directed perpendicular to the vertical jet axis 5 mm downstream the nozzle. Fluorescence was collected with a condenser at cross angles with respect to the jet axis and the laser beam and directed to a photomultiplier FEU-106. The signal was processed with a boxcar-integrator BCI-280 and recorded by a X,Y-recorder.

The saturation curves were measured by recording the signal from the photomultiplier (the fluorescence intensity I_f) to the Y-axis and the signal from the photodiode (the excitation intensity I_e) to the X-axis of the X,Y-recorder. Both signals

were separately analog-processed with an integrator and a logarithmic converter. Continuous attenuation of the excitation intensity was ensured by an absorbing cuvette containing a dye solution with slowly increasing concentration, through which the laser beam was directed. Briefly, the concentrated ethanol solution of 6-aminophenalenon was dropped into the dye pump initially filled with water. To be sure in the linearity of the registration system only one order of the dynamic range of the photomultiplier and the photodiode was used: in case the X-signal decreased more than 10 times, then one of the three filters with about 10% transmission, initially set in front of the photomultiplier and the photodiode, was removed and the right position of the recording pen was restored by adjusting the knobs of the recorder. This procedure was repeated three times in order to cover the whole attenuation range of I_e (four orders of magnitude). Linearity of the detecting system was checked by the X,Y-plot recorded by the same procedure as for saturation curve, but by using the scattered laser light (without jet) instead of the quinizarin fluorescence signal. The X and Y axes were calibrated by neutral filters with known tranmission.

The absolute values of the excitation intensity I_e were determined from the measurements of the laser pulse parameters: pulse energy, its duration and cross-section area of the laser beam. The accuracy of the I_e value (its relative uncertainty was estimated to be a factor of two) was determined mostly by the beam cross-section measurement, by using a burning pattern on the photoplate left after exposition with the laser beam.

2.3 Rotational band contours

Quinizarin is a flat molecule with C_{2v} symmetry (Fig. 2.1). The 0-0 band at 19917 cm^{-1} is the strongest one in the $S_1 \leftarrow S_0$ excitation spectrum [6]. The rotational constants of quinizarin were estimated to be A=0.024 cm^{-1}, B=0.013 cm^{-1}, C=0.0085 cm^{-1} based on the calculated constants for antracene taken from Ref. [5] and standard bond length for =O···H-O- fragments (see Fig. 2.1).

The vibrational structure of the $S_1 \leftarrow S_0$ excitation and dispersed laser-induced fluorescence spectra of jet-cooled quinizarin has been investigated in Refs. [6,7]. In these works the vibrational frequencies, intensities of vibronic bands and supposed mode symmetries are tabulated. Higher resolution of our laser system permitted us to measure also the rotational contours of the vibronic bands in the excitation spectrum.

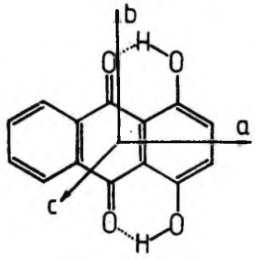

Figure 2.1: The structural formula and the principal inertial axes of quinizarin molecule.

The rotational contour of the 0-0 band measured at different excitation intensities is shown in Fig. 2.2. The P, Q, and R branches and their power-dependent distortion is clearly visible. The distance between the maxima of P and R branches marked by q can be used for the estimation of the rotational temperature T_{rot} in the jet. Considering that $q \approx 2*2BJ_m$, where $J_m = \sqrt{kT_{rot}/B}$ is the approximate J quantum number for the rotational lines from which the maxima of P and R branches are formed (see Chapter 3) and that B is the intermediate rotational constant, we get $T_{rot} \approx q^2/16B$, where T_{rot} is expressed in cm^{-1} units. The measured P,R distance of 1.2 cm^{-1} corresponds to $T_{rot} \approx 10$ K and $J_m \approx 23$.

The unsaturated width of the Q branches of all the 19 bands from 0-0 band up to 0-0+486 cm^{-1} band measured were determined by the spectral bandwidth of the laser ($\Delta\nu$=0.045 cm^{-1}). Such a width of the Q branch implies that the relaxation time of S_1 vibronic levels is longer than $(2\pi c\Delta\nu)^{-1}$= 0.12 ns. Indeed, time resolved measurements [8] have shown a single exponential decay with τ=3.8 ns after excitation into the 0-0 band. Moreover, the

narrowness of the Q branch implies that the upper and the ground state rotational constants are the same within 0.5% and hence the geometric configuration changes but to a little extent on excitation. It can be shown by using the symmetric top (where A>B=C) rotational energy formulas that the residual width of the Q branch due to the difference of the B constants ΔB is approximately $\Delta B J_m^2$. The observed width of the Q branch 0.045 cm^{-1} corresponds to 0.5% upper limit for $\Delta B/B$. The same

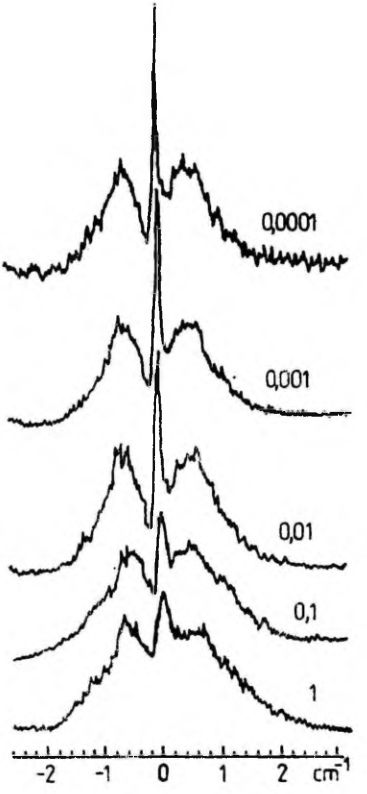

Figure 2.2: Rotational contour of the 0-0 band (19917 cm^{-1}) at different excitation intensities. For each contour the attenuation factor from the full intensity of the laser beam (9.1×10^5 W/cm^2).

upper limit is crudely valid for ΔA: for larger ΔA the K-structure of the rotational spectrum should determine the effective width of the Q branch. The Doppler broadening in a free jet is mainly caused by the variation of the component of the flow velocity along the laser beam, briefly, by diverging the flow [9]. The Doppler width was estimated to be ≈ 0.02 cm^{-1} by using the expression $\Delta\nu_D/\nu=\Delta u/c$, where $u \approx 600$ m/s is the flow velocity of Ar jet and $\Delta u \approx 0.5u$ is its variation.

The vibrational modes of quinizarin are classified according to the irreducible representations of C_{2v} group: there exist 25 totally symmetric a_1 modes, 24 in-plane b_2 modes, 11 out-of-plane b_1 modes, and 12 out-of-plane a_2 modes [7]. The vibronic transitions to a_1 modes in the excitation spectrum are allowed with the transition moment being parallel to the long in-plane axis ($d \parallel a$), because both S_0 and S_1 electronic states have a_1 symmetry. A number of weak bands in the excitation spectrum between 0-0 and 0-0+486 cm^{-1} bands (corresponding to 117, 159, 185, 214, 251, 282, 313, 360, 395, 444, 451, 473 cm^{-1} modes) are assigned in Ref. [6] to forbidden transitions (see Fig. 2.3). These weak transitions are supposed to be induced by Hertzberg-Teller coupling to some upper electronic state with b_1 or b_2 symmetry. If it is indeed so, then these forbidden bands should have transition dipole moment parallel to b- or c-axis (see Fig. 2.1); $d \parallel b$ for b_1 modes or $d \parallel c$ for b_2 modes. a_2 modes are also forbidden within the Herzberg-Teller approximation.

Since the transition dipole moment can only lie parallel to one of the a, b or c principal axes (see Fig. 2.1) because of symmetry restrictions, the rotational spectra of a hybrid type are excluded for quinizarin. If the rotational spectrum is of a pure type (a-type if $d \parallel a$, b-type if $d \parallel b$ and c-type if $d \parallel c$) and the molecular configuration does not change considerably on transition, then the knowing of only the shape of the rotational contour is enough to distinguish b-type spectra from a- or c-type spectra: a- or c-type rotational spectra show a strong Q branch but b-type spectrum has a dip instead of the Q branch in the middle of the contour [5, 10].

From the absence of b-type contours in the excitation

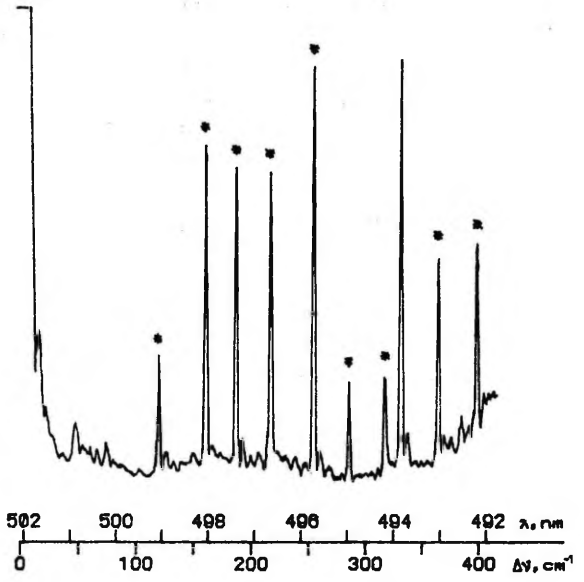

Figure 2.3: A part of quinazarin excitation spectrum. The zero for $\Delta\nu$ corresponds to the 0-0 band. Dipole-forbidden vibronic bands are indicated by asterisks.

spectrum we conclude that all observed forbidden transitions are of c-type and, consequently, induced by out-of-plane b_2 vibrations. Forbidden bands have been assigned to out-of-plane modes also in Ref. [7]. However, in Ref. [6] some of the forbidden bands have been assigned to in-plane b_1 modes, contrary to our results.

2.4 The saturation curves of the 0-0 band

The measured saturation curves (the fluorescence intensity I_f as a function of the excitation intensity I_e) in case of excitation into the P branch of the 0-0 band with an intracavity etalon and without it are presented in Fig. 2.4. Both curves show a transition from linear dependence at a low excitation intensity to sqare root dependence (with twice lower slope in

the logarithmic scale) at high I_e. The nonlinear (superlinear) dependence at low excitation intensities, which occurs also in the case of linearity check with a scattered laser light may be caused by the inclining of the laser beam by thermal lensing effects in the dye used for beam attenuation (see the description of the experiment).

The saturation curves are well described by the formula

$$I_f \propto I_e / \sqrt{1 + I_e/I_{sat}} , \qquad (2.1)$$

where I_{sat} is the saturation intensity. This formula describes the saturation of absorption for excitation with a continuous monochromatic light in case of an inhomogeneously broadened two-level absorbing system according to the theory presented in [11,12]. In case of jet-cooled quinizarin the rotational structure (in addition to the Doppler broadening) plays the

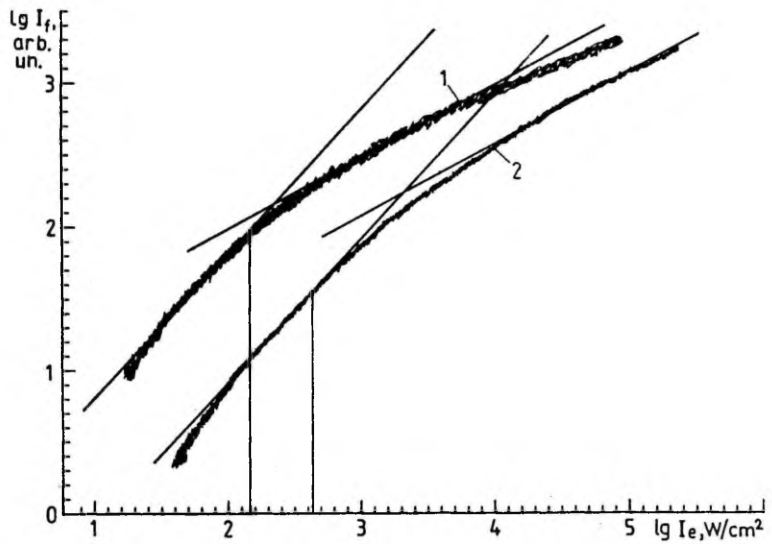

Figure 2.4: The saturation curves (logarithm of the fluorescence intensity as a function of that of the excitation intensity) for excitation into P branch of the 0-0 band contour: 1) laser with etalon (FWHM=0.045 cm^{-1}); 2) without etalon (FWHM=0.25 cm^{-1}). The straight lines represent the linear and sqare root dependence in the low- and high-intensity limit, respectively. The saturation intensities (150 W/cm^2 and 430 W/cm^2) are marked by vertical lines.

role of inhomogeneous broadening: different lines in the band contour come from different rotational states. The least square fitting of the observed saturation curves to Formula (2.1) yields for I_{sat} the values of 150 W/cm^2 (laser with an intracavity etalon) and 430 W/cm^2 (without etalon).

The saturation effect in the case of a single line (without inhomogeneous broadening) is described by

$$I_f \propto I_e / (1 + I_e/I_{sat}) . \qquad (2.2)$$

According to (2.2) at high intensities, $I_e \gg I_{sat}$, the fluorescence intensity I_f (which is proportional to the power absorbed from the laser beam) approaches a constant value, but according to (2.1), where inhomogeneous broadening is taken into account, I_f continues increasing proportional to $\sqrt{I_e}$. This difference has a simple physical explanation: an increasing number of (not completely saturated) neighbouring lines are involved into absorption at high intensities, because of the power broadening of every homogeneous line according to

$$\Delta\nu = \Delta\nu_0 \sqrt{1 + I_e/I_{sat}} , \qquad (2.3)$$

where $\Delta\nu_0$ is the homogeneous linewidth, determined by the Fourier transform of the upper state lifetime: $\Delta\nu_0 = (2\pi c\tau)^{-1}$. The S_1 state 0-level lifetime of 3.8 ns [8] corresponds to the homogeneous width of 1.4×10^{-3} cm^{-1}. The power broadening (of a single line) can be treated as a larger saturation-induced decrease of absorption at small detunings (laser frequency from the absorption resonance) compared to that of large detunings resulting in an effectively broadened absorption lineshape. Although this rate equation treatment ignores coherent effects, a more consistent theory [11] gives the same result (2.3) for power broadening.

The power broadening appears directly in the observed 0-0 band contour as a power-dependent broadening of the Q branch (see Fig. 2.2). The distortion of the whole contour can be modelled by convoluting the unsaturated contour shape (inhomogeneous distribution function) with the power-broadened homogeneous width according to (2.7). The width of the Q branch at $I_e = 10^6$ W/cm^2 estimated by (2.3) is about 0.1 cm^{-1}. Larger value of the observed width (0.4 cm^{-1}) remains still inexplicable.

2.5 Time-dependent and laser mode-structure effects

Though the Formula (2.1) describes the observed saturation curves well enough, the value of I_{sat} obtained by a direct fitting to (2.1) depends on several experimental conditions. In order to get purely molecular parameters (the transition moment for the 0-0 band) it is necessary to estimate also the influence of the factors, which remain beyond the approximations within which the Formula (2.1) has been deduced:

- finite duration of the laser pulse (about 4 ns),
- population loss due to the nonradiative processes and the fluorescence ending at the excited vibrational levels of S_0 after excitation into the 0-0 band ("open" two-level system),
- nonmonochromatic excitation (laser mode structure effects)
- nonuniform intensity distribution in the laser beam (spatial structure of the transversal modes),
- rotational structure instead of spectrally uniformly distributed lines with the same transition probability.

The influence of time-dependent effects in case of pulsed excitation is estimated by solving the rate equations for an open two-level system:

$$\left.\begin{aligned} d\rho_2/dt &= W(\rho_1-\rho_2) - \rho_2/\tau \\ d\rho_1/dt &= W(\rho_2-\rho_1) + \alpha\rho_2 \end{aligned}\right\}, \qquad (2.4)$$

where α is the probability for a ground state population after emitting a fluorescence photon ($\alpha \leq \tau^{-1}$). Initially only the ground state is assumed to be populated: $\rho_2(t=0) = 0$ and $\rho_1(t=0) = 1$. The excitation probability W is modelled by a rectangular pulse with the length t_1 in the time domain, and a Lorenzian with FWHM $\Delta\omega = 1/\tau$ in the frequency domain:

$$W(I_e, t, \omega-\omega_0) = I_e(t) \,/\, 2\,\tau\, I_{sat}\, [1+(2\tau)^2(\omega-\omega_0)^2] \,. \qquad (2.5)$$

Note that I_{sat} is defined so that the double rate of stimulated transitions, 2W, is equal to the decay rate $1/\tau$ if $I_e=I_{sat}$ and $\omega=\omega_0$.

The irreversibly absorbed energy (the absorbed energy without the part returned to the laser beam by stimulated emission) and the total fluorescence yield are proportional to the time-integrated upper state population:

$$F(I_e, \omega-\omega_0) = \int \rho_2(I_e, t, \omega-\omega_0)\, dt \,. \qquad (2.6)$$

In principle $F(I_e, \omega-\omega_0)$ represents the shape of a power-broadened homogeneous line in case of pulsed excitation. This function calculated for $I_e=10^3\ I_{sat}$ (at higher intensities larger deviation from stationary case is expected) is presented in Fig. 2.5 for a closed ($\alpha = \tau^{-1}$) and a completely open ($\alpha = 0$) two-level system (curves 1 and 2 respectively). The case of an open system is the closest to the reality (it will be shown below that only a 0.0017 fraction of S_1 0-level population returns to the same rotational states of S_0 0-level by fluorescence). For both cases the duration of the laser pulse t_l was taken equal to the upper state decay time $t_l=\tau$. The measured values of t_l and τ are 4 ns and 3.8 ns, respectively. Curve 3 in Fig. 2.5 corresponds to the stationary case: a closed system under continuous excitation. In this case $\rho_2(I_e, \omega-\omega_0)$ is presented instead of $F(I_e, \omega-\omega_0)$. Only in the stationary case (1) is exactly valid and the power-broadened lineshape remains Lorentzian [11, 12]. For a quantitative comparison of the pulsed

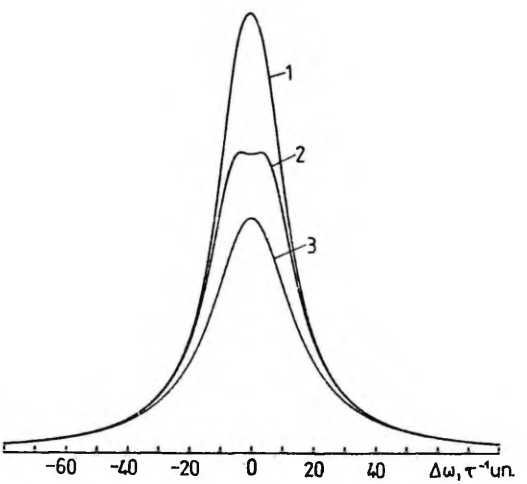

Figure 2.5: Calculated power-broadened homogeneous line shape at the excitation intensity $I_e=10^3 I_{sat}$ for: 1) pulsed excitation and closed 2-level system ($t_l=\tau$ and $\alpha=1/\tau$); 2) pulsed excitation and open system ($t_l=\tau$ and $\alpha=0$); 3) continuous excitation and closed system ($t_l \to \infty$ and $\alpha=1/\tau$).

and the stationary case all three curves are normalized so that their wings overlap, because at large detunings from resonance (or low excitation intensities) the population changes are always linear to I_e.

In case of inhomogeneous broadening the fluorescence yield (or intensity) is expressed as a convolution of $F(I_e, \omega-\omega_0)$ (or $\rho_2(I_e, \omega-\omega_0)$ in the stationary case) with the inhomogeneous distribution function $g(\omega_0)$:

$$I_f \propto \int F(I_e, \omega-\omega_0)\ g(\omega_0)\ d\omega_0 \ . \qquad (2.7)$$

If the inhomogeneous distribution is flat enough ($g(\omega_0) \approx$const), then the fluorescence intensity is simply proportional to the area below the $F(I_e, \omega-\omega_0)$ curve. The rotational contour near the maximum of P branch is sufficiently flat to justify this assumption (the saturation curves were recorded under excitation into the P branch). The fact that the difference of the areas below curves 2 and 3 in Fig. 2.5 being about 1.3, shows that the stationary approximation is valid within 30%. However, it should be noted that for a more correct treatment coherent effects should be taken into account: Bloch equations should be solved.

The pulsed dye laser has generally a multi-mode radiation. Experiments [13], performed on VL-18 laser have shown that within the bandwidth of the laser radiation determined by spectrally selective elements (grating and etalon) several modes occur, whose intensity and spectral position vary occasionally from pulse to pulse. However, the frequency interval between the neighbouring longitudinal modes $\Delta\nu_{mm}=1/2l$, which is determined by the effective resonator length l, remains fixed. For a VL-18 laser l= 26 cm and $\Delta\nu_{mm}=0.02\ cm^{-1}$. Each mode is supposed to have a Fourier-limited width $\Delta\nu_m=2\ln 2/\pi c t_l=0.0037\ cm^{-1}$ for a Gaussian-shaped 4 ns laser pulse. Inside the measured bandwidth of the laser radiation $\Delta\nu_l$ (the average envelope of the modes) there exist about $m=\Delta\nu_l/\Delta\nu_{mm}$ modes: i.e. 13 modes without etalon or 2-3 modes with etalon.

At low excitation intensities I_e, where the interval between modes exceeds the power-broadened homogeneous width $\Delta\nu$, the saturation appears at m (the number of modes) times larger

intensities because all the modes act independently, while each mode shares on the average 1/m part of the measured I_e. Hence also the apparent saturation intensity I_{sat}, measured by fitting the saturation curves to (2.1), should be larger than the real one designated below by I'_{sat}. Indeed, excitation with a larger number of modes (without etalon) results in higher I_{sat} (see Fig. 2.4). In the high I_e limit, where the power-broadened homogeneous line covers the whole laser bandwidth, the excitation can be regarded as monochromatic and (2.1) is again valid. These considerations lead to the following corrected formula for the saturation curve:

$$I_f \propto I_e / \sqrt{1 + I_e/\alpha I'_{sat}}\,, \qquad (2.8)$$

where $\alpha=1$ if $\Delta\nu>\Delta\nu_l$, $\alpha=\Delta\nu_l/\Delta\nu$ if $\Delta\nu_{mm}<\Delta\nu<\Delta\nu_l$, and $\alpha=m$ if $\Delta\nu<\Delta\nu_{mm}$; $m=\Delta\nu_l/\Delta\nu_{mm}$, $\Delta\nu$ is expressed by (2.3) and I'_{sat} is the saturation intensity in case of single-mode excitation. The nonmonochromaticity of each mode can be taken into account by introducing an additional parameter β, depending on the ratio of a single mode and power-broadened homogeneous widths. However, estimations showed that the influence of β is negligible.

The fitting of the saturation curves to the corrected Formula (2.8) yields for I'_{sat} the values 75 W/cm^2 (laser with etalon) and I'_{sat}=140 W/cm^2 (without etalon). These I'_{sat} values are accurate within a factor of two, which is determined mostly by the calibration error of the I_e scale of the saturation curves.

The pattern burnt on a photoplate held cross to the laser beam near the jet showed a nonelementary distribution of the incident light due to transversal modes (an unfocussed beam was used in all experiments). In the following we examine with a simple model the possible influence of a nonuniform spatial excitation intensity distribution on saturation curves. Let there be two regions in the cross-section of the laser beam with the areas S_1 and S_2 (S_1/S_2= a) and the intensities I_{e1} and I_{e2} (I_{e1}/I_{e2}= b), respectively. Let the total area $S = S_1 + S_2$ and the total power $I_e S = I_{e1}S_1 + I_{e2}S_2$ be fixed. The total fluorescence intensity is proportional to $(S_1 I_{f1} + S_2 I_{f2})/S$, where the fluorescence intensities are expressed according to

(2.1), $I_{f1} \propto \sqrt{I_{sat} I_{e1}}$ and $I_{f2} \propto \sqrt{I_{sat} I_{e2}}$, if $I_{e1}, I_{e2} \gg I_{sat}$ is valid. In the linear region (at low I_e) I_f and I_e are always proportional independent of the spatial intensity distribution, therefore only the complete saturation ($I_{e1}, I_{e2} \gg I_{sat}$) is the case of interest. After some substitutions we obtain:

$$I_f \propto (a\sqrt{b}+1)\sqrt{I_{sat} I_e} / \sqrt{(a+1)(ab+1)} = x\sqrt{I_{sat} I_e}, \quad (2.9)$$

where the factor $x = (a\sqrt{b}+1)/\sqrt{(a+1)(ab+1)}$ shows how much the fluorescence intensity differs compared to the case of spatially uniform excitation, where b=1 and, consequently, x=1 . Calculations for estimated parameters a=0.25 and b=10 give x=0.85, hence the effect of transversal modes can be ignored.

Although different rotational lines have different transition strengths according to the rotational selection rules, it can be shown (see the explanation in Chapter 3, part 3.4), that within certain approximations (symmetric top, J≫1, uniform distribution of K and M states) the ensemble-averaged (over all K and M rotational states at fixed J) transition strength is the same for every P, Q, and R branch and for every J states (see Fig. 2.6). Consequently, the shape of the P, Q, and R branches is determined by the density of the rotational lines

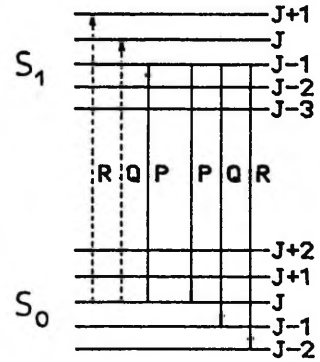

Figure 2.6: Electronic-rotational transitions in case of a symmetrical top molecule. The lines of a particular branch (P, Q, or R) starting from the same J state but different K and M states, coincide because of ΔM=0 and ΔK=0 selection rules. The mean transition strength of these overlapped lines is independent of ΔJ (it is the same for all three branches). Solid arrows represent excitation into the P branch and the subsequent fluorescence.

in the spectrum and the rotational population prior to excitation rather than by differences in the strength of the rotational lines. Therefore, the apparent saturation intensity, being related to the average strength of a number of transitions, does not depend essentially on the spectral position inside the contour. Near the maxima of P and R branches the shape of the contour is also flat enough to be treated as a uniform inhomogeneous distribution.

2.6 Transition strength of the 0–0 band

Now we can use the formula derived for a closed two-level system (with single homogeneous absorption line) to caclulate the transition dipole moment of the 0–0 band:

$$d_0 = \sqrt{9\,\hbar^2 c / 8\pi I'_{sat} T_1 T_2}\,, \qquad (2.10)$$

The energy and phase relaxation times, T_1 and T_2, and the S_1 lifetime τ are assumed to be related to each other by $T_1=T_2/2=\tau$ [14], because no collisions occur during τ (τ=3.8 ns). However, in (2.10) a factor 9 considering the rotational effects is added to the original formula taken from [11]; this factor takes into account the random (isotropic) orientation of the transition dipoles (factor 3) and the distribution of the transition strength to P, Q and R branches (another factor 3). The latter is based on the fact that each rotational state of S_0 is a common starting state for three lines, one line per each P, Q, and R branch if parallel transition (d∥a) for symmetric top is assumed (see Fig. 2.6). Thus the effective saturation intensity for a conceivable ensemble of space-fixed transition dipoles oriented parallel to the electric field vector of the incident laser beam is 9 times less than the I'_{sat} = 75 W/cm^{-2} for the ensemble of freely rotating molecules. The transition dipole moment d_0 of the 0–0 band is calculated to be of 0.74 D. The uncertainty interval is determined by a factor of 1.5: 0.5 D < d_0 < 1.1 D.

The transition moment d_0 can be related to the effective radiative lifetime for fluorescence back to the zero level of S_0 (the sum fluorescence of the P, Q, and R branches) by the well-known formula for the Einstein A coefficient ($A=1/\tau_r$):

$$\tau_{r0}^{-1} = 64\,\pi^4 \nu_0^3 d_0^2 \,/\, 3\,h\,c^3, \qquad (2.11)$$

where ν_0 is the 0-0 band frequency (in Hz). It turns out that τ_{r0} = 740 ns. The ratio of the lifetimes, τ/τ_{r0} = 0.005, represents a part of the population excited to 0-level of S_1 which returns to 0-level of S_0 by fluorescence. It should be noted that to the same rotational levels of S_0 depopulated by the excitation returnes a three times less part (0.0017) of the excited population through one of the three branches of the rotational spectrum. The remainder population loss of S_1 0-level is a result of radiative (fluorescence to vibrationally excited levels of S_0) as well as nonradiative (intersystem crossing to triplet T_1 or internal conversion into S_0 vibronic levels) decay mechanisms. In the dispersed fluorescence spectrum, following excitation into the origin band of quinizarin [6], the fluorescence intensity of the origin band makes about 1/5 of the total fluorescence intensity. Hence the fluorescence quantum yield (the share of radiative processes in the total decay rate) of a free quinizarin molecule is about 0.005*5 = 2.5%.

The strength of the 0-0 band can be characterized besides the transition moment by the oscillator strength

$$f_0 = 8\,\pi^2\, m_e \nu_0 d_0^2 \,/\, 3\,h\,e^2, \qquad (2.12)$$

where e and m_e are the electron mass and the charge, respectively, or by the integral cross-section

$$\sigma_0^i = 8\,\pi^3 \nu_0 d_0^2 \,/\, 3\,h\,c\,. \qquad (2.13)$$

The calulated values are f_0 = 0.005 and $\sigma_0^i = 1.4*10^{-4}$ cm^2/s. Both quantities have the error intervals from half up to twice of their values.

In case of a homogeneously-broadened Lorenzian-shaped absorption line with the width $\Delta\nu$ the integral cross-section σ^i and the peak cross-section are related to each other by

$$\sigma^i = \pi\,\Delta\nu\,\sigma\,c \,/\, 2\,. \qquad (2.14)$$

The peak cross-section characterizes the attenuation of the probe beam tuned into the peak of the absorption line, provided the spectral width of the probe beam is much less than that of the absorption line. The 0-0 absorption band of quinizarin dissolved in hexane has about 400 cm^{-1} width and $3*10^{-17}$ cm^2 (peak) cross-section [4], which correspond to the integral

cross-section of $6*10^{-4}$ cm^2/s being close to our value. For the 0-0 band of a free quinizarin molecule the homogeneous linewidth (the width of single electronic-rotational lines) was determined by the lifetime broadening $\Delta\nu_0=(2\pi c\tau)^{-1}=1.4*10^{-3}$ cm^{-1} and the characteristic peak cross-section for these lines expressed by $\sigma_0=2\sigma_0^i/3\pi c\Delta\nu_0$ was estimated to be of $7*10^{-13}$ cm^2. This value can be experimentally checked by the use of a continuous-wave dye laser tuned into selected rotational lines.

It is well known that saturation leads to a relative enhancement of the weak bands in the excitation spectrum. If all the vibronic bands are saturated ($I_e \gg I_{sati}$, where I_{sati} is the saturation intensity for the band, marked by i) then the intensities of different bands in the excitation spectrum are proportional to their transition moments (instead of being proportional to squared transition moments of the bands), because of the rotational contour effects discussed above. This proportionality ($I_{fi} \propto d_i$) at a fixed excitation intensity $I_e \gg I_{sati}$ obviously follows from (2.1), provided that $I_{sati} \propto 1/d_i^2$ (see (2.10)) and $I_{fi} \propto d_i^2$ in the linear limit ($I_e \ll I_{sati}$). For this reason the saturation effects should be carefully checked to avoid a wrong interpretation of the excitation spectra if molecules with a large oscillator strength are excited with a pulsed (especially focussed) dye laser beam.

References

[1] В.Г.Абрамов, О.В.Константинов, Н.Н.Костин, В.А.Ходовой, ЖЭТФ 53 (1967) 822

[2] А.Е.Трещалов, Изв. АН СССР 48 (1984) 757

[3] A.B.Treshchalov, M.G. Rozman, Opt. Commun. 47 (1983) 262

[4] Т.В.Плахотник, А.М.Пындык, Лазерная спектроскопия сложных молекул, Тез. Докл., Таллинн, 1988

[5] B.W.Keelan, A.H. Zewail, J. Chem. Phys. 82 (1985) 3011.

[6] J.Subbi, Chem. Phys. Lett. 109 (1984) 1

[7] G.Smulevich, A.Amirav, U.Even, J.Jortner, Chem. Phys. 73 (1982) 1

[8] Т.Рейнот, Ю.Субби, Я.Аавиксоо, Изв. АН. ЭССР. Физика. Математика. 36 (1987) 381

[9] D.H.Levy, Ann. Rev. Phys. Chem. 31 (1980) 197
[10] T.Ueda, T.Schimanouchi, J. Mol. Spectry. 28 (1968) 350
[11] В.М.Акулин, Н.В.Карлов, Интенсивные резонансные взаимодействия в квантовой электронике, Наука, 1987
[12] W.Demtröder, Laser Spectroscopy, 2nd corrected printing, Springer, Berlin, 1982 (В. Демтредер, Лазерная спектроскопия, Наука, 1985)
[13] Е.Б.Берик, Статистческие свойства излучения импульсного лазера на красителях, Препринт F-35, Тарту, 1986
[14] O.Svelto, Principles of lasers, 2nd edition, Plenum press, New York, 1982 (О.Звелто, Принципы лазеров, Мир, 1984)

Chapter 3

SATURATION OF THE FLUORESCENCE ANISOTROPY OF THE QUINIZARIN JET

3.1 Introduction

A polarization-sensitive detection of gas-phase molecular absorption and fluorescence under linearly or circularly polarized excitation is a powerful method for the investigation of the effects of free rotation, collisions and external electric or magnetic fields [1-4]. Various parameters describing partial orientation and alignment of the ensemble of molecules can be extracted from these measurements [5]. In the majority of polarization-based measurements diatomic molecules have been studied, because they possess the simpliest possibility for the investigation of the effects influencing on the orientational characteristics of a molecular ensemble [2-4]. In case of large organic molecules showing inhomogeneous spectral congestion in vapour phase it is essential to apply the jet-cooling technique [6] to carry out the polarization measurements in collision-free environment by using the laser excitation into a selected single vibronic band.

The existence of the nonzero stationary fluorescence anisotropy for freely rotating large molecules was theoretically predicted for the first time in Ref. [7] for an ensemble of symmetric tops in the classical limit case. In the same work the theoretical results were compared with the experiment on the vapour of TOPOT (1,4-bis(5-p-tolyloxazol-2-yl)benzene) scintillator. Later the quasiclassical theory was generalized to describe also asymmetric tops [8]. In Ref. [9], both quantum and classical treatment were used to investigate the influence of the intramolecular vibrational-rotational energy transfer on the anisotropy of the noncolliding ensemble of symmetric tops. In a complementary experimental work [10] jet-cooled pyrimidine molecules were used to elucidate the vibrational and rotational effects from fluorescence polarization measurements, while the laser frequency was tuned within the rotational contours of selected vibronic bands.

The decrease of laser-induced fluorescence anisotropy (optical alignment) along with the increase of the excitation intensity for Na_2 vapour was observed and explained in Ref. [11] by a balance between anisotropic optical excitation and collisional relaxation, which tends to restore the equilibrium population in S_0 with isotropic distribution of angular momentum projections. At high excitation intensities the resultant nonequilibrium population of S_0 rotational states compensates partly the optically induced anisotropy resulting in a decreased degree of fluorescence polarization.

The present work, being complementary to the one presented in Chapter 2, aims at investigating the dependence of fluorescence anisotropy on the excitation intensity for jet-cooled quinizarin in case of selective excitation into the P, Q, and R branches of the 0-0 band rotational contour of $S_1 \leftarrow S_0$ transition.

3.2 Experimental

A detailed description of the setup has already been presented in Chapter 2, therefore, only the modifications needed for polarization measurements are described here. In all measurements a VL-18 pulsed dye laser (repetition rate was 5 Hz) with an intracavity etalon (laser line FWHM was $\approx$0.045 cm^{-1}) at a fixed wavelength, tuned into the 0-0 band rotational contour of quinizarin (λ=502.02 nm), was used.

The geometrical arrangement used is depicted in Fig. 3.1. Vertical polarization (along the symmetry axis of the jet, marked by z) of the laser beam was ensured by a Glan prism. The time-integrated undispersed fluorescence was collected along x-direction, perpendicular to the jet axis and the laser beam. A polaroid in front of the photomultiplier was used to select z-polarized (vertically) or y-polarized (horizontally) fluorescence. The anisotropy of fluorescence is expressed, as usual, by the polarization degree

$$p = (I_{fz}-I_{fy})/(I_{fz}+I_{fy}) \quad . \qquad (3.1)$$

A single measured value of the polarization degree was an average of about 2500 single pulse measurements of the z- and

y-polarized fluorescence intensities, I_{fz} and I_{fy}, respectively. The fluorescence signal was recorded on the Y-axis of the X,Y-recorder, while X was the time axis. I_{fz} and I_{fy} were recorded one after another by rotating the polarizer 90° after every 500 laser pulses to avoid a systematic error due to the signal drift. To calculate the polarization degree p the values of I_{fz} and I_{fy} were measured afterwards by a ruler from the obtained plot as the corresponding distances from the 0-signal line. The attenuation of the laser beam was accomplished by using calibrated neutral filters.

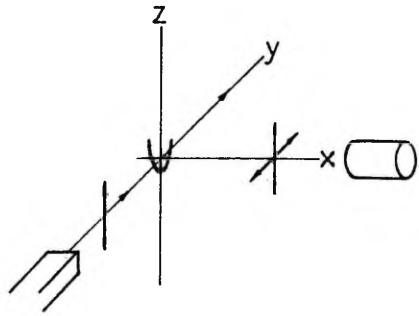

Figure 3.1: Geometrical arrangement of the fluorescence polarization measurements: y- or z-polarized fluorescence following z-polarized excitation along y direction is collected along x direction into the photodetector.

3.3 The observed effects

The experimental values of the polarization degree p are presented in Fig. 3.2 by closed symbols as a function of the logarithm of the relative excitation intensity $\log(I_e/I_{sat})$ in case of excitation into the P, Q, and R branches of the 0-0 band rotational contour (see Fig. 2.1). Three observations were brought out from these measurements:

- excitation into the Q branch (particularly at low I_e values) results in a larger anisotropy compared to the excitation into the P or R branches,
- the anisotropy of the fluorescence decreases if the excitation intensity is raised,

- at high excitation intensities the degree of polarization is a nonzero constant, being the same for each of P, Q, and R branches.

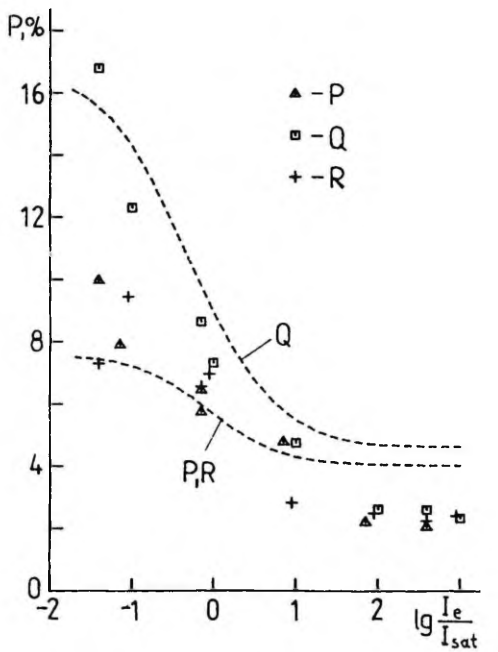

Figure 3.2: Fluorescence polarization degree p as a function of the excitation intensity for excitation into P, Q, and R branches of the 0-0 band rotational contour. I_{sat} =150 W/cm^2 is assumed. Relative error of experimental points along $\lg(I_e/I_{sat})$ scale is 0.1 and along p scale, 0.2 if $\lg(I^e/I^{sat})\approx -1$ and 0.1 for all the other points. Theoretical results are presented by dashed curves.

3.4 Model calculations

In order to explain these phenomena, model calculations aimed at simulating the dependence of the polarization degree on the excitation intensity, were performed. The real jet containing quinizarin molecules we describe for simplicity by an ensemble of symmetric tops with rotational constants

satisfying A/2=B=C and being the same for S_0 and S_1 electronic states. The estimated rotational constants are A=0.024 cm^{-1}, B=0.013 cm^{-1}, and C=0.0085 cm^{-1} (see Chapter 2). The rotation is then characterized by wave functions $|J,K,M\rangle$, where the rotational quantum numbers J, K, and M characterize the total angular momentum and its projections to molecular a-axis and laboratory z-axis, respectively; $-J \le K, M \le J$. For quinizarin the transition dipole moment is parallel to a-axis (d∥a); see Chapter 2. As the a-axis is assumed to be the top symmetry axis, the selection rules are ΔK=0 and ΔM=0 for linearly polarized excitation. The selection rules for the J quantum number, giving rise to P, Q, and R branches, are ΔJ=-1, 0, and 1, respectively.

Next we take into consideration that the estimated mean rotation period $t=2\pi/\overline{I/kT}=70$ ps is much less than the S_1 lifetime $\tau=3.8$ ns. Here $I=h/8\pi^2cB$ is the inertial momentum corresponding to the rotational constant B=0.013 cm^{-1} and T=10 K is the rotational temperature. The duration of a single turn t is roughly the stabilization time of the fluorescence polarization anisotropy to a stationary value. As $t \ll \tau$, the transient effects can be excluded and we can confine oneself taking into account only the stationary rotational $|J,K,M\rangle$ states, which allows us to use the well-known (quantum-averaged) rotational transition probabilities (Hanle-London factors) for the symmetric top.

The intensity of i-polarized fluorescence (i = z, y) is expressed, as in [91], by

$$I_{fi} = \sum_{J,K,M} W_{ez}(\Delta J, J, K, M)\; n(J,K) \sum_{\Delta J=-1}^{1} W_{fi}(\Delta J, J, K, M) \;, \qquad (3.2)$$

where W_{ez} is the effective (considering the saturation) absorption (or excitation) probability for z-polarized light; n is the initial thermal population of S_0 rotational levels; W_{fi} is the probability of fluorescence with z- or y-polarization. The sum over ΔJ (over P, Q, and R branches) takes into account that total undispersed fluorescence is detected. The sum over J, K, and M represent averaging over an ensemble of different rotational states of S_0.

The rotational transition probabilities $W_i(\Delta J, J, K, M)$ for

absorption and fluorescence from $|J,K,M\rangle$ state is determined by the sum of squared nonzero matrix elements of the scalar product of the transition dipole moment and the field strength $d*E=\cos\angle(d,E)=\cos\angle(a,z)$ in the $|J,K,M\rangle$ basis [12]. The probabilities $W_i(\Delta J,J,K,M)$ for x-, y- and z-polarization are presented in Table 3.1, based on the matrix elements taken from [12]. The sum over J in Formula (3.2) includes only the J states which take part in absorption.

Table 3.1: Rotational transition probabilities for the parallel transition ($\Delta K=0$) of the symmetric top

Branch, ΔJ	Polarization, ΔM	$W(\Delta J,J,K,M)$	$W(\Delta J,u,v)$ if $J\gg1$; $u=M/J$, $v=K/J$
Q, 0	z, 0	$\frac{M^2K^2}{J^2(J+1)^2}$	u^2v^2
P, -1	z, 0	$\frac{(J^2-M^2)(J^2-K^2)}{J^2(4J^2-1)}$	$(1-u^2)(1-v^2)/4$
R, 1	z, 0	$\frac{[(J+1)^2-M^2][(J+1)^2-K^2]}{2J^2(J+1)^2}$	
Q, 0	x or y, ±1	$\frac{[J(J+1)-M^2]K^2}{2J^2(J+1)^2}$	$(1-u^2)v^2/2$
P, -1	x or y, ±1	$\frac{[J(J-1)+M^2](J^2-K^2)}{2J^2(4J^2-1)}$	$(1+u^2)(1-v^2)/8$
R, 1	x or y, ±1	$\frac{[J(J+3)+M^2+2][(J+1)^2-K^2]}{2(J+1)^2(2J+1)(2J+3)}$	

The initial equilibrium population of the rotational states is determined by the Bolzmann distribution:

$$n(J,K) \propto (2J+1)*\exp(-E/kT), \qquad (3.3)$$

where 2J+1 -fold M-degeneracy is taken into account and $E = BJ(J+1)+(A-B)K^2$ is the rotational energy of a symmetric top. Distribution (3.3) plotted as a function of the J quantum number determines also the shape of the P and R branches. As regards the shape of rotational branches, one can ignore the $(A-B)K^2$ term and sum the $n(J,K)$ expression over the K states, because the rotational lines starting from different K states are approximately overlapped due to the $\Delta K=0$ selection rule

(see also Fig. 2.6) [13]. This procedure results in a merely J-dependent function with an additional 2J+1 factor: $n(J) \propto (2J+1)^2 \cdot \exp[-BJ(J+1)/kT]$, whose maximum corresponds to $J=\sqrt{kT/B}$ if $J \gg 1$ is assumed. Hence the maxima of P and R branches come from the rotational states with J quantum numbers close to $J_m=\sqrt{kT/B}$. An estimation for $B=0.013$ cm^{-1} and $T=10$ K yields $J_m=23$, thus the high-J-approximation ($J \gg 1$) is justified. This approximation enables one to simplify the expressions of transition probabilities (see Table 3.1). Furthermore, the sums over M and K in (3.2) can be replaced by integrals over continuous variables defined by $u=\cos\theta_M=M/J$ and $v=\cos\theta_K=K/J$, where $-1 \le u, v \le 1$.

Concerning the fluorescence ansotropy the K dependence of the initial rotational population cannot be ignored yet. Considering that $J \gg 1$ and presuming that the rotational constants satisfy $A/2=B=C$, we obtain from (3.3): $n(J,v) \propto \exp[-BJ^2(1+v^2)/kT]$. This expession shows that the population of K states at thermal equilibrium is nonuniform (depends on $v=K/J$) or, in other words, the angular distribution by θ_K is anisotropic. In this case of prolate top the states with $\theta_K \to \pi/2$ or with $v \to 0$ are more populated, hence the total angular momentum J is preferentially perpendicular to a-axis ($J \perp a$). The population of degenerate M states is assumed to be uniform; this means an isotropic orientation of J vectors with respect to the laboratory z-axis. For the J states in the vicinity of the maxium of the rotational branch excited into ($J \approx J_m$) the factor BJ^2/kT is close to unity. This enables a further simplification of the population term: $n(v) \propto \exp(-v^2)$. As not a single term after the sum sign in (3.2) depend any longer directly on J, the sum over J is omitted in the following calculations.

The effective excitation probability W_{eff}, which takes into account the saturation in case of inhomogeneous broadening, is expressed by

$$W_{eff}(\Delta J, u, v) = W_z \,/\, \sqrt{1 + I_e W_z / I'_{sat}}\,, \qquad (3.4)$$

where W_z is the excitation probability from Table 3.1 and I'_{sat} is the saturation intensity of a nonrotating molecule in case the transition moment is parallel to the electric vector of the

exciting field: d‖E. I'_{sat} is related to the measured saturation intensity by $I'_{sat}=I_{sat}/9$, as discussed in Chapter 2. Indeed, it can be shown that the transition probability averaged over (uniformly distributed) K and M states $W_{av,i}=\int\int W_i(u,v)\,du\,dv \,/\, \int\int du\,dv$, where both u and v run from -1 to 1, is always equal to 1/9 for every of i= x, y, or z polarization and for every of P-, Q-, or R-type transition.

The above-mentioned approximations lead eventually to the following expressions of I_{fz} and I_{fy} for calculating the polarization degree:

$$\left.\begin{aligned} I_{fz}&=\int_0^1\int_0^1 c\,[(1-u^2)(1-v^2)/2 + u^2v^2]\,\exp(-v^2)\,du\,dv\,, \\ I_{fy}&=\int_0^1\int_0^1 c\,[(1+u^2)(1-v^2)/4 + (1-u^2)v^2/2]\,\exp(-v^2)\,du\,dv\,, \end{aligned}\right\} (3.5)$$

where

$$c=(u^2v^2) \,/\, \sqrt{1+\alpha\,u^2v^2}$$

in case of excitation into the Q branch and

$$c=(1-u^2)(1-v^2) \,/\, 4\sqrt{1+\alpha\,(1-u^2)(1-v^2)}$$

in case of excitation into P or R branches; $\alpha=9\,I_e/I_{sat}$.

The integrals (3.5) were calculated by using a BASIC-language computer program based on Simpson method. The theoretical curves of the fluorescence polarization degree p (in per cents) as a function of the excitation intensity are plotted with the dotted lines in Fig 3.2. The saturation intensity I_{sat} was taken to be equal to 150 W/cm^2 in the calculations of p; the laser mode effects, the account of which yields a smaller value of I_{sat}, were ignored for simplicity (see Chapter 2). The asymptotic values of the polarization degree in the $I_e \ll I_{sat}$ limit are calculated to be of 16.6% for the Q branch and of 7.6% for the P or R branches. In the opposite limit $I_e \gg I_{sat}$ respective calculated values are 4.7% and 3.9%. Ignoring the initial K-anisotropy (the factor $\exp(-v^2)$) gives larger anisotropy for the Q branch but smaller for the P or R branches: 22.2% and 5.9% in case of $I_e \ll I_{sat}$ and 9.1% and 2.4% in case of $I_e \gg I_{sat}$, respectively.

3.5 Interpretation of the results

Larger anisotropy resulting from excitation into the Q

branch compared to that from P- or R-excitation have a clear explanation. According to the selection rules shown in Table 3.1 the rotational states with $|M|,|K| \to J$ or $\theta_M, \theta_K \to 0$ are preferentially selected by Q excitation but the states with $|M|,|K| \to 0$ or $\theta_M, \theta_K \to \pi/2$ by P or R excitation with z-polarized light. In the case of free rotation of the symmetric top molecule the symmetry axis a (and the transition moment d‖a) precesses around the total angular momentum vector J as depicted in Fig. 3.3. J vector itself remains space-fixed because of the angular momentum conservation law. It is obvious from Fig. 3.3 a that if $\theta_M, \theta_K \to 0$, the molecule rotates so that the total angular momentum vector J and the transition moment remains nearly parallel to z-axis resulting in a larger anisotropy of fluorescence. On the contrary, for the rotational states with $\theta_M, \theta_K \to \pi/2$ the transition moment deviates largely from z-axis during the rotation (see Fig 3.3 b).

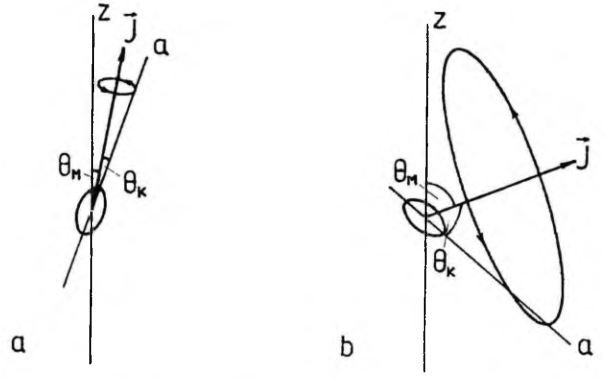

Figure 3.3: Graphic representation of the free rotation of the symmetric top molecule. The angular momentum vector J forms an angle θ_M with the vertical laboratory frame axis z and an angle θ_K with the symmetry axis of the molecule (a-axis). In the rotational states characterized by the small angles θ_M and θ_K the precession of a-axis around the J vector changes the direction of the transition moment (d‖a) to a little extent (a), contrary to the case of nearly right angles θ_M and θ_K (b).

The saturation of the fluorescence anisotropy can easily be

explained by an ensemble of space-fixed isotropically distributed transition dipoles as an example. In the unsaturated limit $I_e \ll I_{sat}$ the absorption probability is always $\propto \cos^2\theta$ (see Fig. 3.4 a); the angle θ is defined by $\theta = \sphericalangle(\mathbf{d}, \mathbf{E}) = \sphericalangle(a, z)$. The corresponding fluorescence polarization degree p amounts to 50%. In case of homogeneous broadening (single line) the effective absorption probability $W_{eff} = \cos^2\theta / (1 + I_e \cos^2\theta / I_{sat})$ approaches a constant value and, hence, the optical induced anisotropy vanishes to zero in the limit $I_e \gg I_{sat}$. Physically this means that all the dipoles, except only those lying exactly parallel to the horizontal plane, are excited (see Fig. 3.4 b). In case of inhomogeneous broadening $W_{eff} = \cos^2\theta / \sqrt{1 + I_e \cos^2\theta / I_{sat}}$, which gives $W_{eff} \propto \cos\theta$ in the $I_e \gg I_{sat}$ limit (see Fig. 3.4 c). The remaining angular dependence (p=1/3 in this case) is a result of the involvement of incompletely saturated neigbouring lines into the absorption by the power-broadening effect.

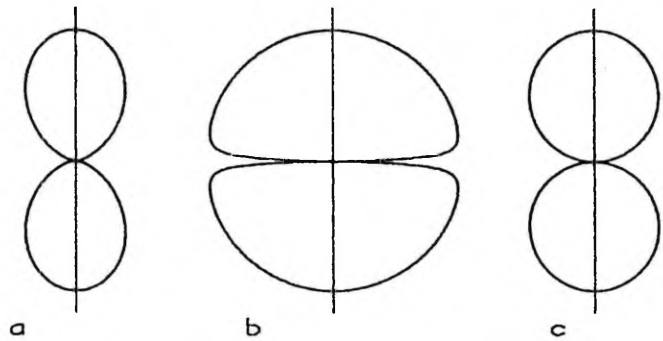

Figure 3.4: Polar diagrams representing the absorption probability for an ensemble of randomly oriented space-fixed dipoles: a) in the unsaturated limit; b) for a single homogeneous line, $I_e/I_{sat} = 10^3$; c) for inhomogeneous broadening, $I_e/I_{sat} = 10^3$. The exciting light beam is assumed to be polarized along the vertical axis.

The same experimental value of the polarization degree for all the P, Q, and R branches at high excitation intensities is explicable by the contribution of the neighbouring P and R lines involved into absorption in case of Q excitation.

The initial distribution of M states, which characterizes anisotropy with respect to the laboratory frame, was assumed to be uniform. However, the alignment of the ensemble along the jet axis has experimentally been observed for some diatomic molecules (I_2, Na_2) [14]. In principle, the resultant initial anisotropy (the M-anisotropy induced by collisions in the beginning of jet expansion together with the K-anisotropy of the thermal population) can be determined by measuring the polarization degree of fluorescence (3.1) in case of excitation with x-polarized light. The optically induced part of the measured anisotropy is then zero because of x-symmetry of the optically excited molecular ensemble. It should be noted that, according to the theory, the alignment of both M and K states is nessecary to get a nonvanishing degree of polarization; isotropy of one of the M or K manifold gives unpolarized fluorescence.

It should also be noted that all the above discussion is about an ensemble of freely rotating molecules. The fluorescence anisotropy would be suppressed to zero if the collision frequency would be much larger than the inverse excited state lifetime of molecule being probed.

References

[1] П.П.Феофилов, Поляризованная люминесценция атомов, молекул и кристаллов, ГИФМЛ, 1959 (P.P.Feofilov, The Physical Basis of Polarized Emission, Consultants Bureau, New York, 1961)

[2] R.N.Zare, Angular Momentum, John Wiley & Sons, New York, 1988

[3] W.Demtröder, Laser Spectroscopy. 2nd corrected printing, Springer, Berlin, 1982 (В.Демтредер, Лазерная спектроскопия, Наука, 1985)

[4] М.П.Аузиньш, Р.С.Фербер, УФН. 160 (1990) 73

[5] A.J.Bain, A.J.McCaffery, J. Chem. Phys. 80 (1984) 5883

[6] D.H.Levy, Ann. Rev. Phys. Chem. 31 (1980) 197

[7] А.П.Блохин, В.Н.Кнюкшто, В.А.Толкачов, Изв. АН СССР, Сер.Физ. 42 (1978) 359

[8] А.П.Блохин, В.А.Толкачов, Опт. и спектр., 51 (1981) 278
[9] G.M.Nathanson, G.M.McClennand, J. Chem. Phys. 81 (1984) 629
[10] G.M.Nathanson, G.M.McClennand, J. Chem. Phys. 84 (1986) 3170
[11] R.E.Drullinger, R.N.Zare, J. Chem. Phys. 51 (1969) 5532
[12] C.H.Townes, A.L.Shawlow, Microwave Spectroscopy, McGraw-Hill, New York, 1955 (Ч.Таунс, А.Шавлов, Радиоспектроскопия, ИЛ, 1959)
[13] В.М.Акулин, Н.В.Карлов, Интенсивные резонансные взаимодействия в квантовой электронике, Наука, 1987
[14] M.P.Sinha, C.D.Caldwell, R.N.Zare, J. Chem. Phys. 61 (1974) 491

Chapter 4

$S_1 \leftrightarrow S_0$ SPECTRA OF JET-COOLED BENZIMIDAZOLE AND BENZOTRIAZOLE

4.1 Introduction

The near-UV singlet-singlet absorption transitions of benzo-derivatives of five-membered heterocycles, including indole, benzimidazole and benzotriazole, are $\pi^* \leftarrow \pi$ type transitions to two excited electronic states, S_1 and S_2, labelled by ^1L_a and ^1L_b, according to the suggestion of Platt [1]. Such a labelling permits the distinguishing of these two states. According to the usual group-theoretical labelling both states are totally symmetric and therefore indistinguishable, because the only symmetry element for these molecules is the plain where the atoms lie. Both transitions are dipole allowed because of their in-plane transition dipole moments [2].

Among these molecules the most thoroughly studied one is indole. Its weaker ^1L_b transition with the oscillator strength f=0.01 has a dominant 0-0 band (origin) and short Franck-Condon progressions of a few modes, but the ^1L_a (f=0.07) transition forms a broad band with a hardly noticable vibrational structure in the absorption spectrum. The origins of ^1L_a and ^1L_b states may lie close in energy, although the absorption maximum of ^1L_a state lies 3000 cm^{-1} above the ^1L_b origin [2-4]. The ^1L_b origin of gas-phase indole is located at 35233 cm^{-1} [5]. A large amount of recent experimental work has been devoted to finding out spectral and temporal manifestations of the near-lying ^1L_a state for jet-cooled indole, substituted indoles and their complexes with various solvents (see Refs. [6-9] and references therein). On the grounds of experiments and quantum chemical calculations [10] it can be concluded that ^1L_b state exhibits a locally excited character but ^1L_a state, a charge transfer character.

The room-temperature UV absorption, fluorescence, phosphorescence spectra and respective polarization spectra of benzimidazole and benzotriazole solutions with various solvents have been measured and analyzed in Ref. [2]. Benzimidazole

shows a structured ^1L_b band and a broad ^1L_a band whose origin lies about 4000 cm^{-1} higher than ^1L_b origin. For benzotriazole the opposite ordering of ^1L_a and ^1L_b states has been found: ^1L_a origin lies about 4000 cm^{-1} lower than that of ^1L_b state. Both absorption bands are broad and smooth; however, the fluorescence coming from ^1L_a state exhibits a clearly-visible vibrational structure [2]. Vibrational structure of the vapour-phase $S_1 \leftarrow S_0$ absorption spectrum of benzimidazole has been investigated in Ref. [11]. Rotational constants of benzimidazole and benzotriazole have been determined by a 0-0 band contour analysis of the vapour absorption spectra in Refs. [12] and [13], respectively. The data concerning the ground-state vibrations derived from Raman and IR spectra have been summarized in Ref. [14] for benzimidazole and in Ref. [15] for benzotriazole.

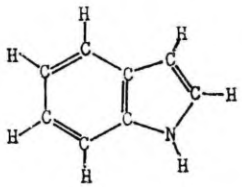

INDOLE

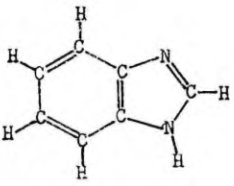

BENZIMIDAZOLE

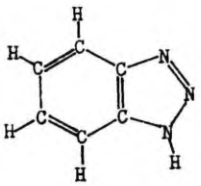

BENZOTRIAZOLE, 1H-TAUTOMER

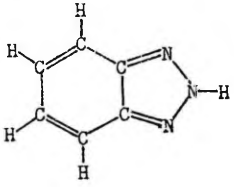

BENZOTRIAZOLE, 2H-TAUTOMER

Figure 4.1: The structural formulae of indole, benzimidazole, and two tautomers of benzotriazole: 1H-tautomer with C_s-symmetry and 2H-tautomer with C_{2v}-symmetry.

An important peculiarity of benzimidazole and benzotri-

azole is proton tautomerism [16]. Both molecules have two identical tautomers (1H and 3H); benzotriazole can form, in principle, also a 2H-tautomer (Fig. 4.1). However, experimentally only the 1H-tautomer of benzotriazole has been observed in the crystalline phase [17]. In solution the equilibrium mixture of both tautomers may exist [16]. The problem is analogous in the case of 1,2,3-triazole molecule, where only 2H-tautomers are observable in the gas phase, while in solution both tautomers have been found [18].

The present work is aimed at obtaining spectroscopic information about isolated benzimidazole and benzotriazole molecules, especially about the proton tunnelling or transfer effects in excited states. This paper includes also the results of our previous work about benzotriazole [19], the spectra being recorded once more with a better resolution. The influence of mode-mixing effects and the nature of the first excited state (^1L_a versus ^1L_b) on the observed excitation and single-vibronic-level dispersed fluorescence spectra will be discussed.

4.2 Experimental

Although the melting point of benzotriazole (98°C) is much lower than that of benzimidazole (172°C), the oven temperature for benzotriazole was kept at a higher value (160°C) than for benzimidazole (140°C) in order to increase its weaker fluorescence signal. The mixture of the sample vapour with the Ar carrier gas (typical pressure 20 kPa) was continuously expanded into vacuum through a 0.2 mm orifice. The vacuum of 0.2 Pa was maintained with a 700 l/s booster pump NVBM-0.5 backed by a 5 l/s rotary pump 2NVR-5D. No differences were found in the excitation spectra after twofold recrystallization of the samples from ethanol; therefore commercially available chemicals without any additional purification were used afterwards.

Fluorescence was excited with a frequency-doubled dye laser VL-22, pumped by an ELI-73 excimer laser at a repetition rate of 5 Hz. A frequency-doubled unfocussed dye laser beam (diameter 1 mm, FWHM 0.4 cm^{-1}, pulse energy 40 μJ) crossed the jet 5

mm downstream the nozzle. The excitation spectra were obtained by measuring the total undispersed emission. The dispersed fluorescence spectra were measured by one half of a DFS-24 0.82 m double monocromator in the second order of the 1200 grooves/mm grating. The aperture angle of the collecting optics (the ratio of the lens diameter to its distance from the jet) was 3/3.5 for the undispersed emission and 5/18 for the dispersed emission. In both cases the signal was detected by a UV photomultiplier FEU-106, processed by a boxcar-integrator BCI-280 and recorded with a chart-recorder.

Dye laser wavelength counter was calibrated by using a Fe/Ne hollow cathode lamp and an auxiliary monochromator (MDR-23). The calibration procedure was as follows: at first the monocromator was tuned to a selected Ne emission line, then the scattered laser radiation was directed into the monocromator and the dye laser wavelength was ajusted to the maximum transmission of the monocromator; after that the difference of Ne line wavelength and the reading of the dye laser wavelength counter were written down. This procedure was repeated with every next Ne reference line until all the wavelength region of interest was covered. During the measurements the wavelength marks generated by the dye laser controller or by the dispersing monocromator circuitry were recorded on a paper sheet together with the spectrum. Such a calibration technique guaranteed a ± 2 cm^{-1} uncertainty of band wavenumbers (in UV) in the excitation spectra. For the fluorescence spectra the precision of band wavenumbers was determined mostly by the width of the slits (the resolution) of the dispersing monochromator.

The excitation spectra were not normalized to laser intensity. In these spectra strong bands may have partly been affected by saturation effects. The dispersed fluorescence spectra were normalized to the total fluorescence signal. Some of the fluorescence spectra are quite noisy due to photon statistics of a weak signal. No cut-off filters were used to discriminate against the scattered laser radiation. For the resonance fluorescence signal the amount of scattering was found to be neglible for the 0-0 band of benzimidazole and

about 20% for the 0-0 band of benzotriazole, in case the laser beam was accurately aligned. However, for weaker bands the contribution from scattering could be considerably larger.

4.3 Benzimidazole

4.3.1 Excitation and 0-0 band fluorescence spectra

Figure 4.2 shows the $S_1 \leftarrow S_0$ fluorescence excitation spectrum of benzimidazole. The data obtained from this spectrum are presented in Table 4.1. Some hot sequence bands (with intervals 11, 52, 63 and 138 cm^{-1}) appeared torwards the red of a very strong 0-0 band at 36032 cm^{-1}, because of insufficient cooling in our continuous Ar jet. In the absorption spectrum of benzimidazole vapour [11] strong sequences emerge from these bands. The hot bands are assigned to the 1←1 vibronic transitions of low-frequency out-of-plane modes. In the far infrared spectrum of indole [20] three such vibrations were observed: out-of-plane deformation of the five-membered ring (189 cm^{-1}), butterfly mode (206 cm^{-1}), and out-of-plane deformation of the benzene ring (415 cm^{-1}). The pattern of hot bands is well repeated for the fundamentals up to 729 cm^{-1}. For hot bands associated with higher-frequency fundamentals the intervals (particularly the 11 cm^{-1} one) are perturbed by mode-mixing effects.

Figure 4.3 shows a dispersed fluorescence spectrum following the excitation into the 0-0 band. The ground-state vibrational frequencies up to 1700 cm^{-1} determined from this spectrum and correlated with the ones from infrared, Raman and solid state fluorescence data from [14] are summarized in Table 4.2. The similarity of band intensities in our 0-0 band fluorescence spectrum and in that of solid benzimidazole from [14] helped us greatly to correlate the bands; however, some uncertainties remain. The 1079 cm^{-1} band is tentatively correlated with the 1138 cm^{-1} NH in-plane bending mode observed in crystalline benzimidazole. A large frequency shift can be explained by hydrogen bonding in the solid phase. The band at 1395 cm^{-1} is too strong to be attributed to the 776+620 cm^{-1} combination band only; therefore, this band may correspond to

the 1412 cm^{-1} fundamental in the fluorescence spectrum of the solid. Some weak bands at 433, 852 and 1424 cm^{-1} are correlated to IR and Raman bands for which out-of-plane symmetry was established. Their existence can be explained in terms of the Hertzberg-Teller coupling. The out-of-plane symmetry of the strong 1360 cm^{-1} band is still doubtful. For shortness only the assignments of a few stronger combination bands are included

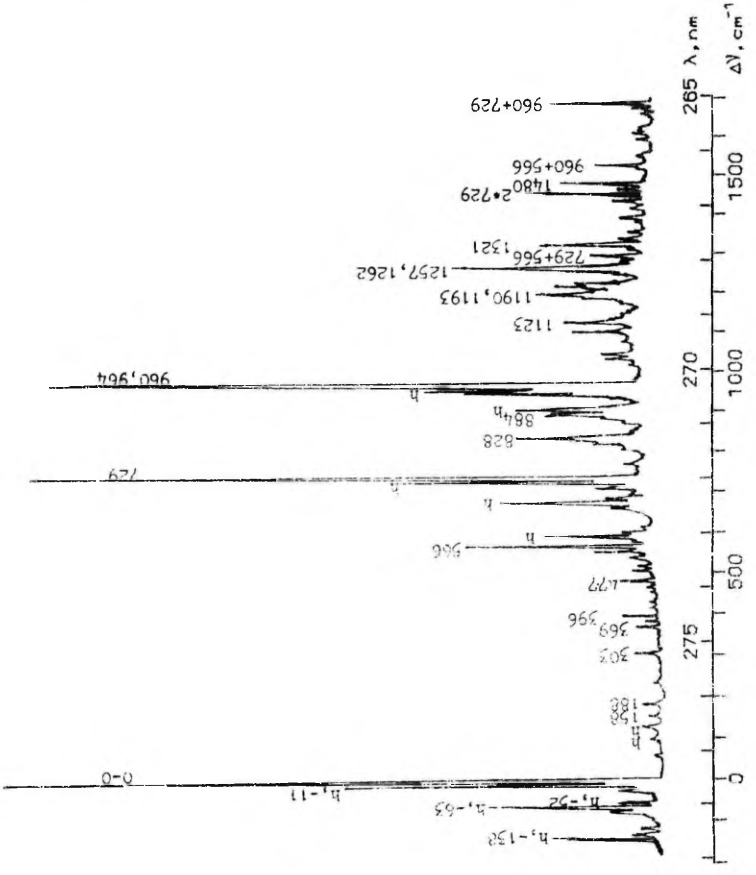

Figure 4.2: Fluorescence excitation spectrum of benzimidazole. The zero for $\Delta\nu$ corresponds to the 0-0 band.

Table 4.1: Assignments of the excitation spectrum of benzimidazole. Accuracy is ±2 cm^{-1}. Hot bands are marked by h, fundamentals by f and uncertain assignments by ?.

$\Delta\nu(cm^{-1})$	I	assignment	$\Delta\nu(cm^{-1})$	I	assignment
-138	m	h	1032	w	(729+303) ?
-76	w	h, -63-11	1041	w	
-63	m	h	1092	m	
-52	w	h	1123	m	(729+396) ?
-23	w	h, -2*11	1133	vw	
-11	s	h	1173	vw	
0	vs	origin	1190	m	
158	vw	f	1193	m	
188	vw	f	1216	m	
237	vw		1221	m	
303	w	f	1257	s	
369	w	f	1262	s	f
384	vw	h, 396-11	1276	vw	
396	w	f	1291	w	(729+566)
414	vw	h, 477-63	1310	vw	
462	vw	h, 477-11	1321	m	f
477	w	f	1339	w	
501	vw	h, 566-63	1343	w	
514	vw	h, 566-52	1361	vw	(960+396) ?
538	vw		1381	vw	
555	w	h, 566-11	1395	w	
566	s	f	1420	vw	
593	m	h, 729-138	1437	vw	(960+477) ?
651	w	h, 729-63-11	1449	w	
665	m	h, 729-63	1459	m	2*729
677	w	h, 729-52	1469	w	
700	w	h, 729-2*11	1480	m	
715	s	h, 729-11	1531	w	(960+566)
729	vs	f	1556	vw	
767	vw		1562	vw	
828	m	f	1611	vw	
884	m	f	1624	vw	
895	m	h, 960-63	1661	vw	
923	vw		1676	vw	
936	s	f	1691	m	(960+729)
944	s	h, 960-11	1700	vw	
960	vs	f			
964	s				

into Table 4.2, though most of these bands are assigned. The frequencies of the ground and the excited state fundamentals agree well with the ones determined from the vapour-phase absorption spectrum [11]. However, in the vapour-phase spectrum the 36023 cm^{-1} feature assigned to the 0-0 band in Refs. [11,12], may actually be a sequence band.

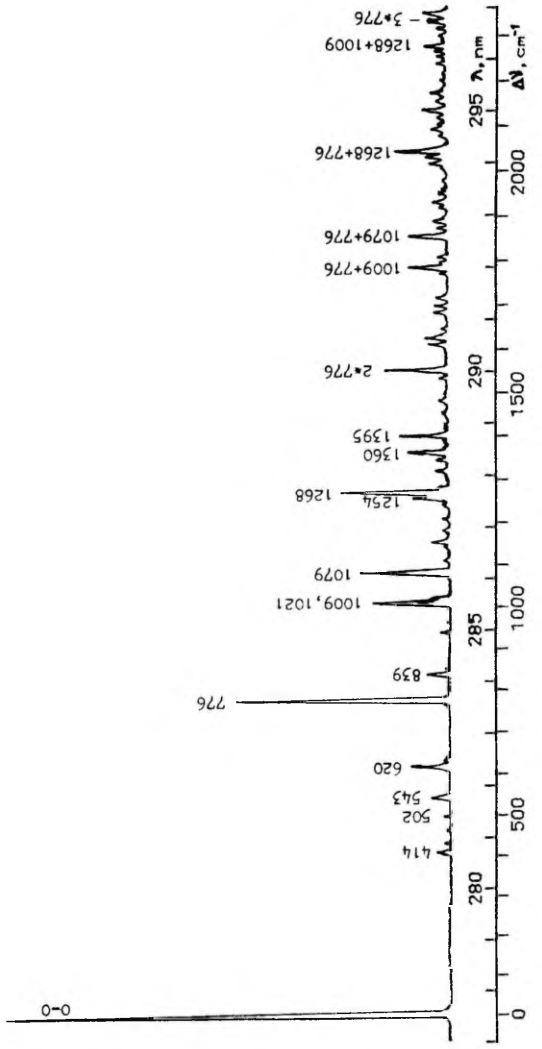

Figure 4.3: Dispersed fluorescence spectrum of benzimidazole excited into the 0-0 band. Resolution 0.045 nm (6 cm^{-1}). The zero for $\Delta\nu$ corresponds to resonance fluorescence; $\Delta\nu>0$ indicates shifts to the red.

Table 4.2: Frequency shifts of the bands of the dispersed 0–0 band fluorescence spectrum of jet-cooled benzimidazole together with the Raman, infrared and fluorescence data of solid benzimidazole, and symmetry assignments for fundamentals from [14]. The relative intensity, I, is shown for the jet and the solid state fluorescence data.

jet fluor. $\Delta\nu(cm^{-1})$	I	IR $\nu(cm^{-1})$	Raman $\Delta\nu(cm^{-1})$	solid fluor. $\Delta\nu(cm^{-1})$	I	assignment
0	400					
414	6	419		419	1	a'
433	5	424	422			a"
467	1					
502	7					
543	17	544	547	542	7	a'
620	36	619	620	617	16	a'
776	190	772	780	777	86	a'
839	21	837				
852	8	848	851	849	3	a"
869	5					
939	10	950	962	963	2	a'
1009	82	1006	1008	1003	34	a'
1021	15					
1052	2					
1079	75	1138	1139	1138	35	a'
1115	2	1115	1112			a'
1154	18	1155	1160	1159	5	a'
1183	4	1185	1191	1193	4	a'
1207	6	1200	1206			a'
1240	8					2*620
1254	46	1250	1251			a'
1268	102	1263	1277	1277	100	a'
1297	2	1295	1306			a'
1318	13					(776+543)
1344	8		1349			a'
1360	38	1360	1368	1365	6	a"
1395	44	1410	1414	1412	13	a' &(776+620)
1429	3		1421			a"
1458	8	1460	1463			a'
1482	7	1485	1481			a'
1498	4		1500			a'
1535	4					
1552	45			1549	11	2*776
1612	10					(776+840)
1631	18	1620	1623	1621	9	a' &(1009+620)
1699	10					(1079+620)
1785	34					(1009+776)
1852	33					(1079+776)
2043	42					(1268+776)
2277	22					(1268+1009)
2347	28					(1268+1079)

4.3.2 Fluorescence from the vibronic levels of S_1

In order to find out a correspondence between the excited and the ground state modes the fluorescence spectra of the strongest excited state fundamentals were recorded. In the case of a good overlap between the excited and the ground state wave functions the strongest feature in the dispersed fluorescence spectra following the excitation into the upper state vibronic levels is the band corresponding to the $\Delta v=0$ ($1\rightarrow1$) vibronic transition, which serves as the origin for the other bands forming a spectrum resembling the one resulting from 0-0 excitation. The distance between the $\Delta v=-1$ (resonance fluorescence) and the $\Delta v=0$ bands is the frequency of the ground state mode sought for (see Refs. [21,22]). The ground state counterparts of the excited state modes up to 729 cm^{-1} determined in this way are given in Table 4.3. The 433, 467 and 635 cm^{-1} modes in the fluorescence spectrum following the excitation into the 0-0+303 cm^{-1} band, are probably out-of-plane modes mixed with one another by the Dushinsky effect.

Excitation into the hot sequence bands associated with the 0-0 band yields spectra similar to the 0-0 band dispersed fluorescence but shifted to an apparent origin (the resonance band) due to the difference in out-of-plane mode frequencies for S_0 and S_1. Only for the -138 cm^{-1} hot band a very weak extra band in fluorescence, shifted by 210 cm^{-1} to the blue from the resonance band, was detected.

Excitation into the bands higher than 800 cm^{-1} above the 0-0 band produced a pattern of bands in the $\Delta v=0$ region in emission, whose complexity increases with the excitation energy. The frequency intervals and the relative intensities for stronger bands in the $\Delta v=0$ region are listed in Table 4.3. Figs. 4.4, 4.5 and 4.6 show the fluorescence spectra following the excitation into the 960, 964, and $2*729$ cm^{-1} bands above the S_1 origin, respectively.

The complexity of the fluorescence patterns in the $\Delta v=0$ region of spectra, which increases together with the density of vibrational states, indicates that the fluorescence comes from the level (or a number of overlapped levels) representing a superposition of several zero-order vibrational states coupled

Table 4.2: Frequency shifts of the bands of the dispersed 0–0 band fluorescence spectrum of jet-cooled benzimidazole together with the Raman, infrared and fluorescence data of solid benzimidazole, and symmetry assignments for fundamentals from [14]. The relative intensity, I, is shown for the jet and the solid state fluorescence data.

jet fluor. $\Delta\nu(cm^{-1})$	I	IR $\nu(cm^{-1})$	Raman $\Delta\nu(cm^{-1})$	solid fluor. $\Delta\nu(cm^{-1})$	I	assignment
0	400					
414	6	419		419	1	a'
433	5	424	422			a"
467	1					
502	7					
543	17	544	547	542	7	a'
620	36	619	620	617	16	a'
776	190	772	780	777	86	a'
839	21	837				
852	8	848	851	849	3	a"
869	5					
939	10	950	962	963	2	a'
1009	82	1006	1008	1003	34	a'
1021	15					
1052	2					
1079	75	1138	1139	1138	35	a'
1115	2	1115	1112			a'
1154	18	1155	1160	1159	5	a'
1183	4	1185	1191	1193	4	a'
1207	6	1200	1206			a'
1240	8					2*620
1254	46	1250	1251			a'
1268	102	1263	1277	1277	100	a'
1297	2	1295	1306			a'
1318	13					(776+543)
1344	8		1349			a'
1360	38	1360	1368	1365	6	a"
1395	44	1410	1414	1412	13	a' &(776+620)
1429	3		1421			a"
1458	8	1460	1463			a'
1482	7	1485	1481			a'
1498	4		1500			a'
1535	4					
1552	45			1549	11	2*776
1612	10					(776+840)
1631	18	1620	1623	1621	9	a' &(1009+620)
1699	10					(1079+620)
1785	34					(1009+776)
1852	33					(1079+776)
2043	42					(1268+776)
2277	22					(1268+1009)
2347	28					(1268+1079)

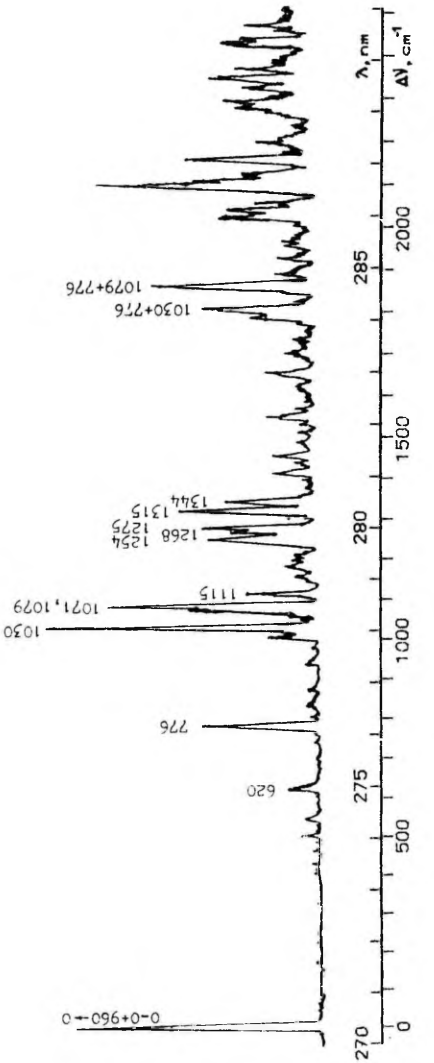

Figure 4.4: Dispersed fluorescence spectrum of benzimidazole excited into the 0-0+960 cm^{-1} band (the 'bright' component of 960; 964 cm^{-1} Fermi-resonance doublet of S_1). Resolution 0.068 nm (9 cm^{-1}).

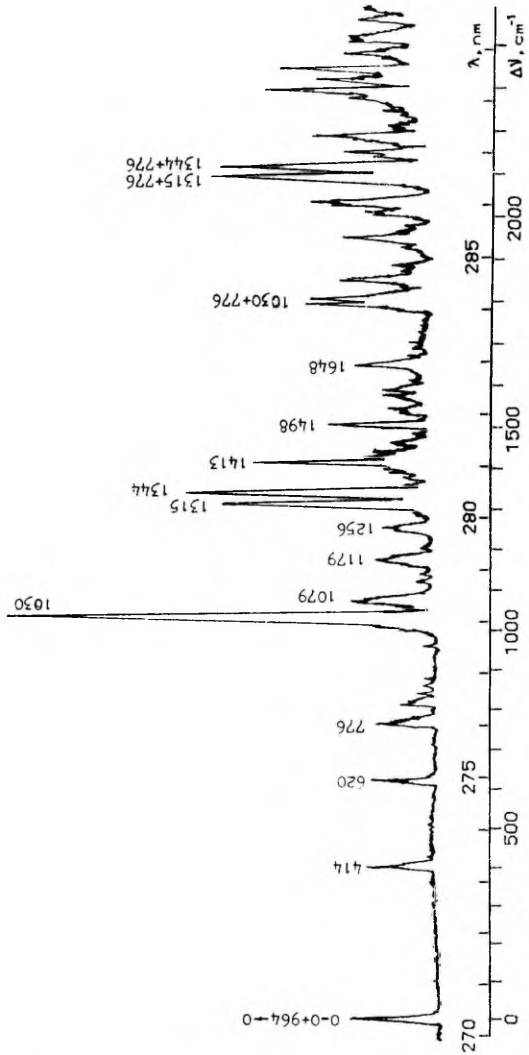

Figure 4.5: Dispersed fluorescence spectrum of benzimidazole excited into the 0-0+964 cm^{-1} band (the 'dark' component of 960; 964 cm^{-1} Fermi-resonance doublet of S_1). Resolution 0.09 nm (12 cm^{-1}).

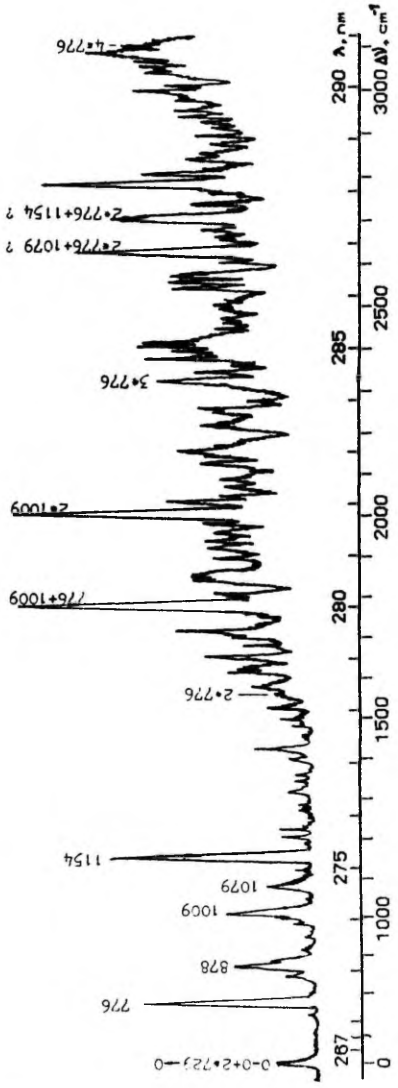

Figure 4.6: Dispersed fluorescence spectrum of benzimidazole excited into the 0-0+2×729 cm^{-1} overtone band of the breathing mode. Resolution 0.14 nm (18 cm^{-1}). Note the scale gap.

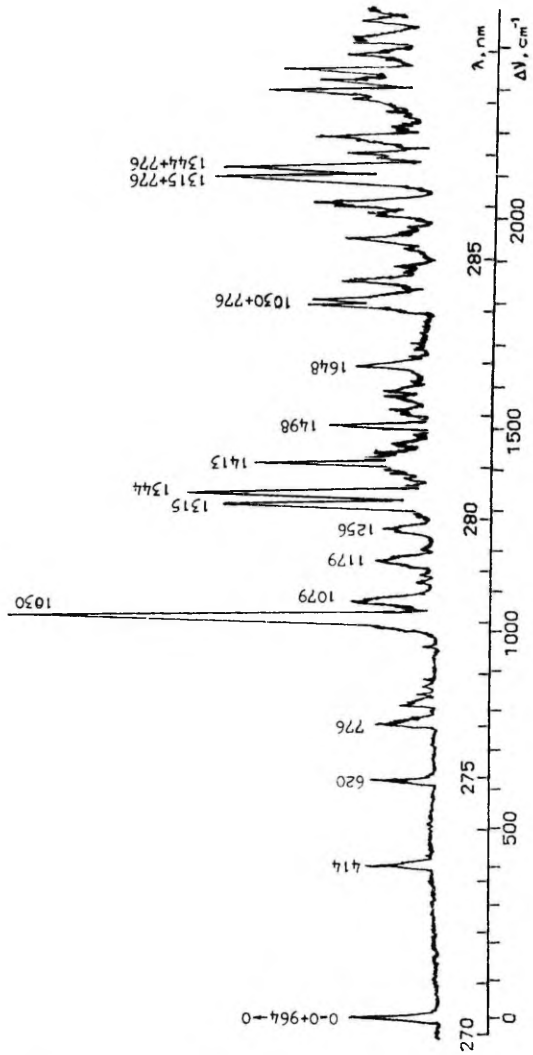

Figure 4.5: Dispersed fluorescence spectrum of benzimidazole excited into the 0-0+964 cm^{-1} band (the 'dark' component of 960; 964 cm^{-1} Fermi-resonance doublet of S_1). Resolution 0.09 nm (12 cm^{-1}).

(or 2) quanta in the breathing mode of S_1 and end in levels of S_0 with up to 4 breathing quanta combined with excitation of all other active S_0-modes. For the 0-0+729 cm^{-1} band this is actually the case, only the 776+1145 cm^{-1} combination band being anomalously strong. However, the dispersed fluorescence spectrum of the 0-0+2*729 cm^{-1} band (Fig. 4.6) contains in addition to the zero-order band pattern other bands due to mode mixing (the strongest are the 1154, 776+1009 and 2*1009 cm^{-1} bands) and an almost continuous background located to the red from 278.5 nm. Due to anharmonic couplings the 2*776+1079 and 2*776+1154 cm^{-1} combination bands are relatively strong although the 2*776 cm^{-1} band is very weak. The appearance of the continuous background indicates that IVR begins to have effect at 1450 cm^{-1} above the S_1 origin.

Table 4.4: Franck-Condon analysis of the 776; 729 cm^{-1} breathing mode of benzimidazole. Calculated squared FC factors for the distortion parameter γ=0.7 are compared with the observed relative intensities (in parentheses) of relevant bands in fluorescence spectra excited into 0-0, 0-0+729 and 0-0+2*729 cm^{-1} bands.

v'	v"				
	0	1	2	3	4
0	0.61 (0.62)	0.29 (0.29)	0.08 (0.07)	0.02 (0.02)	
1	0.31 (0.25)	0.16 (0.15)	0.32 (0.34)	0.16 (0.16)	0.05 (0.04)
2	0.07 (0.08)	0.37 (0.33)	0.01 (0.03)	0.24 (0.24)	0.20 (0.29)

4.4 Benzotriazole

4.4.1 Excitation spectrum

Figure 4.7 shows the $S_1 \leftarrow S_0$ fluorescence excitation spectrum of jet-cooled benzotriazole. The observed bands are listed in Table 4.5. All the bands located to the red from the strong 0-0 band (34927 cm^{-1}) are attributed to hot sequence bands, because their intensity relative to that of 0-0 band decreases when Ar pressure is raised. Two hot bands at -566 and -540 cm^{-1} from

the origin are supposed to be 0←1 vibronic transitions originating from the 566 and the 540 cm^{-1} ground state modes, respectively, because they are too far away from the 0–0 band. Some of the hot bands are assigned to 566 cm^{-1} red shifted repetitions of the cold 1←0 bands located in the 500 cm^{-1} region based on their similar relative intensities. Hence they represent 1←1 transitions starting from the 566 cm^{-1} vibration of S_0. Some hot bands may naturally belong to the 1←1 transitions of out-of-plane modes.

A quick onset of the congestion of bands towards the blue in the exitation spectrum hints to strong anharmonicity of the upper state potential. Above 1200 cm^{-1} from the 0–0 band only a weak and broadened band, assigned to the 795+481 cm^{-1} combination band, appears. The rapid intensity decline indicates an effective coupling to some nonradiative manifold. The continuation of the absorption towards the blue is clearly visible in the absorption spectrum of benzotriazole in solution [2].

4.4.2 Vibrational analysis of S_1 origin fluorescence

The low-resolution dispersed fluorescence survey spectrum of benzotriazole excited to 0–0 band is presented in Fig. 4.8. The same spectrum taken with a better resolution is shown in Fig. 4.9. Its 90 nm extent and its intensity maximum lying in the centre implies a large change in geometric configuration on S_1-S_0 electronic excitation. The frequencies and assignments of the observed bands are shown in Table 4.6. We had no success in correlating the observed fundamentals in our spectrum with the IR and Raman bands known from solution spectra [15], because of large discrepancies between the frequencies and intensities of the bands. Only the strong 540 cm^{-1} band seems to correspond to the Raman band of the same frequency. If it is indeed so, then the 540 cm^{-1} mode cannot be triazole ring torsion as suggested in [15]; it must be an in-plane mode, provided that benzotriazole is planar in both S_0 and S_1 states. The 783 cm^{-1} breathing mode, which forms strong band in the Raman and the IR spectra, does not appear in our 0–0 band fluorescence spectrum. Also, the lack of 566 cm^{-1} band is surprising, because in the exitation spectrum there exist both the -540 and the -566 cm^{-1}

hot band.

An analysis of the higher-frequency part of the 0-0 band dispersed fluorescence spectrum (Table 4.6) revealed that it is dominated by the combination bands of strong 540, 1153, 1242, 1405, and 1447 cm^{-1} fundamentals. It shold be noted that the

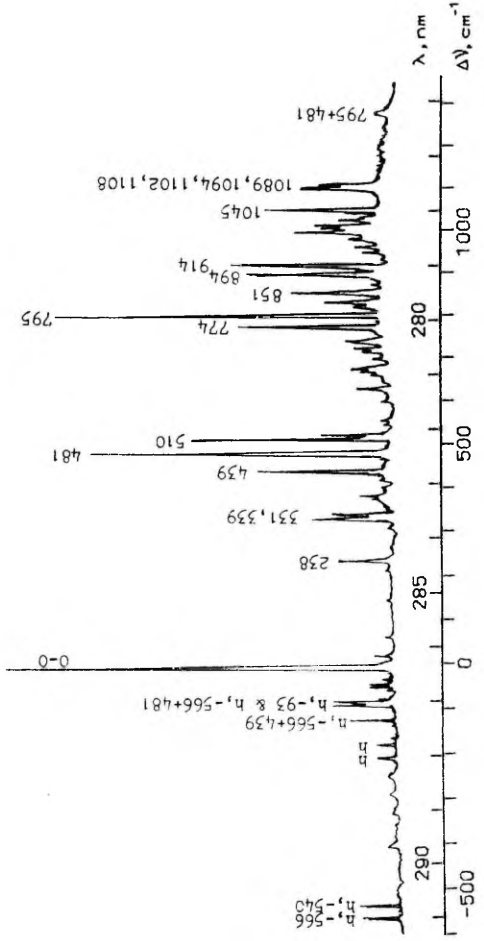

Figure 4.7: Fluorescence excitation spectrum of benzotriazole.

Table 4.5: Assignments of the fluorescence excitation spectrum of benzotriazole. Accuracy ±2 cm^{-1}.

$\Delta\nu(cm^{-1})$	I	assignment	$\Delta\nu(cm^{-1})$	I	assignment
-566	m	h	716	vw	
-540	m	h	721	w	
-210	w	h	740	w	
-183	w	h	774	s	
-127	m	h, -566+439	795	vs	
-93	m	h	828	w	
-86	m	h, -566+481	851	m	
-59	w	h, -566+510	894	s	
-49	w	h, -566+519	914	s	
0	vs	origin	947	vw	
24	w	h	959	w	2*481
67	vw	h, -566+633	974	w	
238	m		988	m	(510+481)
331	m		998	m	(519+481)
339	m		1006	m	
374	w		1018	w	2*510
381	w		1045	s	
439	s		1089	m	
481	vs		1094	m	
510	s		1102	m	
519	m		1108	m	
633	w		1274	vw	(795+481)
655	vw				
663	w				
679	w				

band assigned to 1405+1127 cm^{-1} combination is surprisingly strong, nevertheless the 1127 cm^{-1} band is relatively weak and does not form any strong combination with the 1242 cm^{-1} band. A comparison of the 0-0 band fluorescence spectra in Figs. 4.8 and 4.9 reveals that the strong features in the low-resolution spectrum are formed by a number of bands coinciding within the spectral resolution of the monochromator, while the intensity of some single band is generally weaker than that of resonance fluorescence. The intensity maximum lies in the region where 3 vibrational quanta of 1153, 1242, 1405, and 1447 cm^{-1} modes combine. The third overtones of these vibrations are already very weak compared to the combination bands. This means that on electronic transition the geometric configuration of benzotriazole shifts along several normal coordinates, but not along the coordinate of a single mode as stated in our previous work [19].

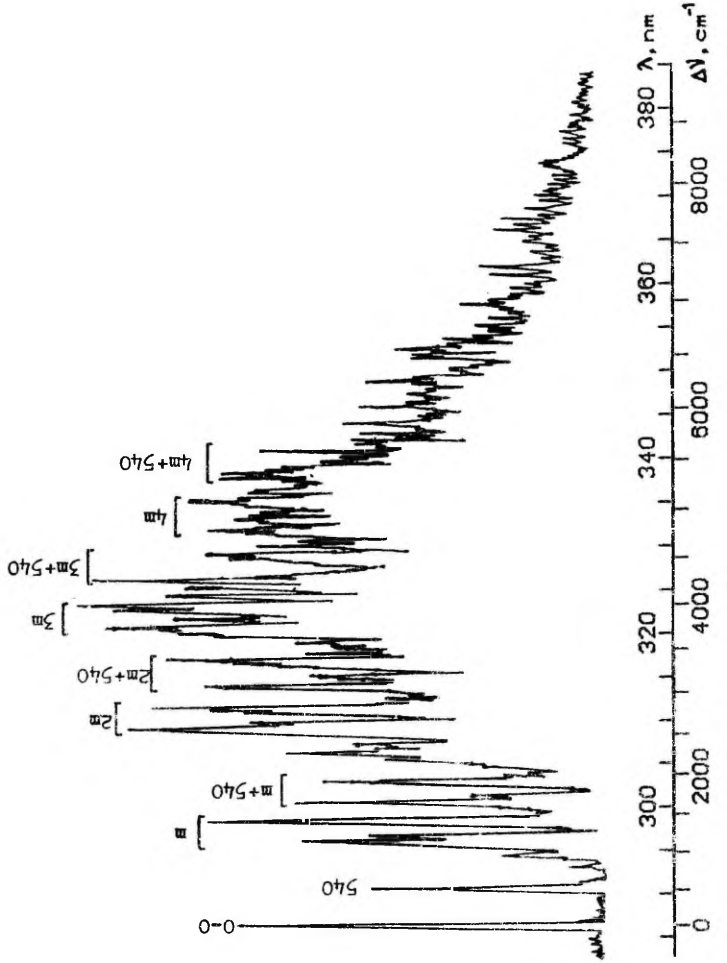

Figure 4.8: Dispersed fluorescence spectrum of benzotriazole excited into the 0-0 band. Low resolution, 0.45 nm (43 cm^{-1}). The 1153, 1242, 1405, and 1447 cm^{-1} modes together are labelled by m (see Fig. 4.9).

Table 4.6: Assignments of the dispersed origin fluorescence spectrum of benzotriazole. The spacings $\delta\nu$ between successive combination bands involving the 1405 and the 1447 cm^{-1} mode are listed to demonstrate the influence of anharmonicity.

$\Delta\nu(cm^{-1})$	I	assignment	$\Delta\nu(cm^{-1})$	I	assignment	$\delta\nu(cm^{-1})$
0	vs		2484	m	2*1242	
540	s	f	2528	s	(1405+1127)	32
590	vw	f	2560	s	{(1447+1127)	
626	w	f			|(1405+1153)	39
836	vw	f	2599	s	(1447+1153)	
963	w	f	2646	s	(1405+1242)	42
998	w	f	2688	s	(1447+1242)	
1078	w	2*540	2778	s	(2235+540)	
1127	m	f	2807	s	2*1405	41
1153	s	f	2848	vs	(1447+1405)	36
1192	w	f	2884	m	2*1447	
1242	s	f	2982	w	(2444+540)	
1374	w	f		...		
1405	vs	f	3429	m	(2884+540)	
1447	vs	f	3488	m		
1511	w	(963+540)	3572	m		
1536	w	(998+540)	3641	s	(2*1242+1153)	
1633	w		3685	vs	(1405+1153+1127)	
1664	m	(1127+540)	3719	s	(1405+2*1153)	34
1691	s	(1153+540)	3753	s	(1447+2*1153)	
1727	vw	(1192+540)	3792	vs	(1405+1242+1153)	48
1779	s	(1242+540)	3840	s	(1447+1242+1153)	
1943	s	(1405+540)	3898	m	(1405+2*1242)	34
1984	s	(1447+540)	3932	vs	(1447+2*1242)	
2066	w		3970	vs	(2*1405+1153)	29
2122	m		3999	vs	(1447+1405+1153)	
2205	w	(1242+963)	4094	s	(1447+1405+1242)	33
2235	m	(1242+998)	4128	m	(2*1447+1241)	
2272	m		4255	s	(1447+2*1405)	33
2315	m	2*1153	4288	s	(2*1447+1405)	
2336	m		4331	s	(3792+540)	
2389	m	(1242+1153)		...		
2410	m		4828	m	(4288+540)	
2444	w		5083	s	(3932+1153) ?	
			5129	m	(3970+1153) ?	

We tried to simulate the 0-0 band fluorescence spectrum in the framework of a model of independent (parallel) harmonic oscillators [27]. The intensities (squared Franck-Condon factors) of the fundamentals and the overtones of each mode were taken proportional to $\gamma^{2v}/v!$, where γ is the distortion parameter and v is the number of quanta for the corresponding mode. The intensities of combination modes were calculated as products of the intensities of fundamentals from which they are

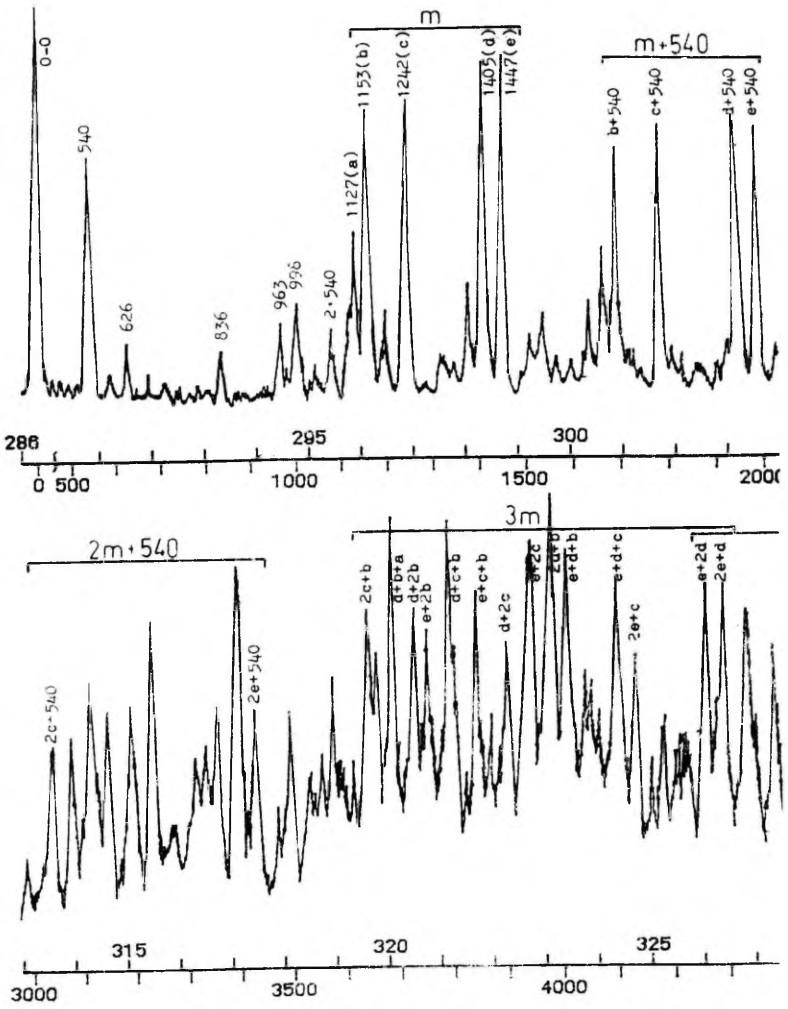
0-0
540
626
836
963
996
2·540
1127(a)
1153(b)
1242(c)
1405(d)
1447(e)
m
m+540
b+540
c+540
d+540
e+540
286
295
300
0 500
1000
1500
2000
3m
2m+540
2c+540
2e+540
2c+b
d+b+a
d+2b
e+2b
d+c+b
e+c+b
d+2c
e+d+b
e+d+c
2e+c
e+2d
2e+d
315
320
325
3000
3500
4000

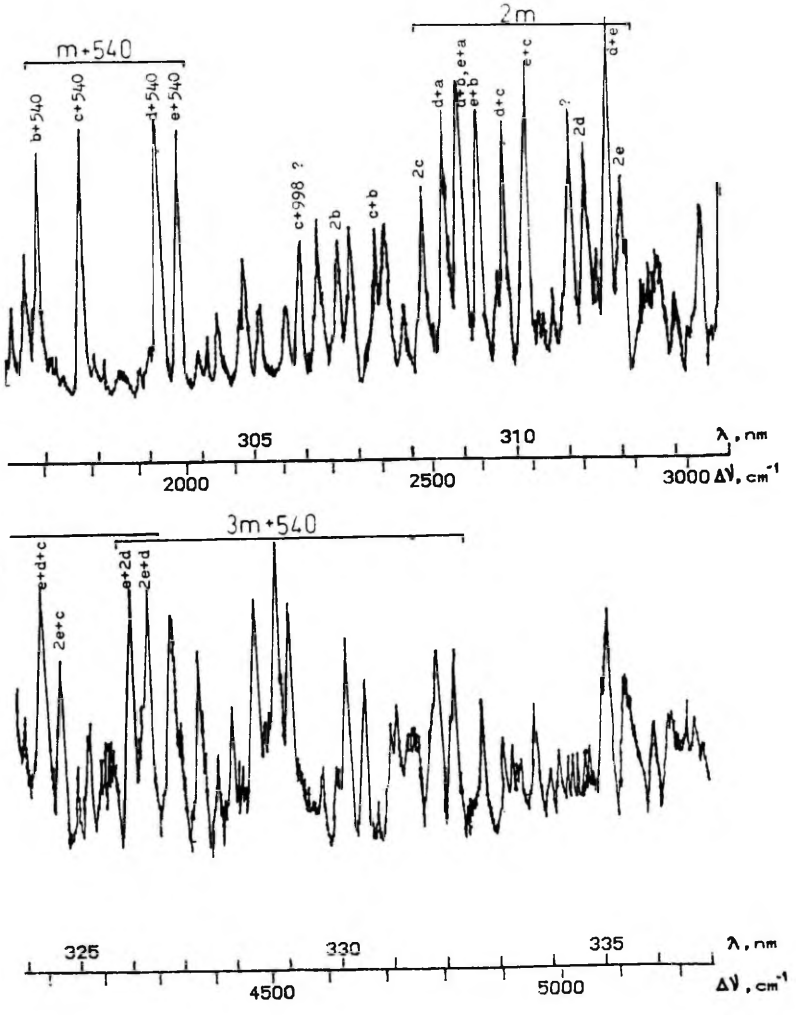

Figure 4.9: Dispersed fluorescence spectrum of benzotriazole excited into the 0-0 band. High resolution, 0.14 nm (13 cm^{-1}). Note the scale gap.

made up. A qualitative resemblance with the experimental spectrum was obtained with a set of distortion parameters 0.85, 0.95, 0.95, 1.0 and 1.0 for 540, 1153, 1242, 1405 and 1447 cm^{-1} modes, respectively. We did no go on with a more refined modelling because the measured intensities of the bands are poorly reproducible due to the weak signal strength.

In the third column of Table 4.6 the frequency differences of combination modes in the pairs made up by combining the 1405 cm^{-1} and 1447 cm^{-1} fundamentals with the same set of other modes are listed. These level spacings are well reproduced also between the respective combinations with 540 cm^{-1} mode. The variation of these spacings is explained by anharmonic coupling effects (Fermi resonances). It should be noted that only static couplings can influence the fluorescence spectrum resulting from the 0-0 band excitation.

The dispersed fluorescence spectrum following the excitation into the 0-0+481 cm^{-1} band is shown in Fig. 4.10. The

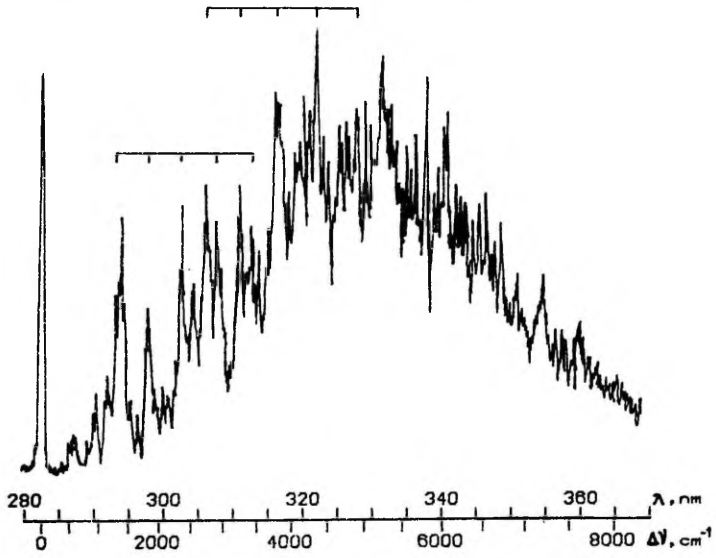

Figure 4.10: Dispersed fluorescence spectrum of benzotriazole excited into the 0-0+481 cm^{-1} band. Resolution 0.54 nm (51 cm^{-1}). Two progressions of 540 cm^{-1} mode are indicated.

Table 4.7: Assignments of the strongest features in the dispersed fluorescence spectrum of benzotriazole excited to the 0-0+481 cm^{-1} band. Many features assigned to fundamentals are also observed in the 0-0 band fluorescence spectrum.

$\Delta\nu(cm^{-1})$	I	assignment
0	s	
430	w	f
540	w	f, 540
670	w	f
980	m	f, 963 & f, 998
1160	m	f, 1153
1320	s	f
1420	s	f, 1405 & f, 1447
1860	m	(1320+540)
2400	s	(1320+2*540)
2760	vs	(1320+1420)
2840	vs	2*1420
2940	vs	(1320+3*540)
3300	vs	(1420+1320+540)
3490	vs	(1320+4*540)
3840	vs	(1420+1320+2*540)

frequencies of some features determined from this spectrum are listed in Table 4.7. Unlike the 0-0 spectrum, the 540 cm^{-1} band is weak, but there exists a long progression (up to v=4) of the 540 cm^{-1} mode is built on the 1320 cm^{-1} band. Two progressions of the 540 cm^{-1} mode are marked in Fig. 4.10. Mode mixing by the Dushinsky effect may be responsible for such a modification of the spectrum: the formation of a long single-mode progression at certain mixing parameters has theoretically been predicted in [28]. Thus, we cannot state firmly that the 481 cm^{-1} mode is the upper state counterpart of the 540 cm^{-1} mode.

4.5 Conclusions about the excited electronic states

The first excited state of benzimidazole has been assigned to ^1L_b and that of benzotriazole, to ^1L_a on the basis of solvent shifts and fluorescence polarization measurements of the corresponding solutions [2]. We retained the same assignments for isolated molecules. Short progressions and a very strong 0-0 band in the excitation spectrum and the fluorescence spectrum from S_1 origin in the case of benzimidazole point to a good Franck-Condon overlap between S_0 and S_1 (^1L_b) wave

functions. Only the breathing mode forms a somewhat longer progression. On the contrary, the overlap of S_0 with the S_1 (^1L_a) wave function for benzotriazole is poor: an analysis of the fluorescence spectrum following the excitation into the 0-0 band indicates that the ground-state equilibrium configuration differs strongly from that of the excited state along the normal coordinates of several modes.

The geometric configuration and atomic masses of benzimidazole, benzotriazole and also indole are quite similar; therefore, close vibrational frequencies are expected to be observed in the spectra of these molecules. A tentative correlation between some low-frequency in-plane modes marked by a, b, c and d is established for these three molecules in Table 4.8. In the excitation and the 0-0 band fluorescence spectra of benzimidazole and indole b and c modes are intense, but in the spectra of benzotriazole a and d modes dominate. The prominence of particular modes in absorption and emission is related to certain changes of molecular geometry on electronic transition, which in turn depends on the the excited state wave function (^1L_a or ^1L_b). Moreover, in a recent study two-photon excitation of jet-cooled indole with linearly and circularly polarized light permitted one to distinguish the ^1L_a and ^1L_b type of vibronic bands [7]. It appeared that the vibronic bands of a

Table 4.8: Frequency shifts (in cm^{-1}) and relative intensities of the bands belonging to the modes marked by a, b, c and d, in the excitation spectra (S_1 state data) and in the 0-0 band fluorescence spectra (S_0 state data) of indole, benzimidazole and benzotriazole: for benzotriazole ^1L_a-character modes (a and d) dominate, but for benzimidazole and indole ^1L_b-character modes (b and c) are more intense.

mode	indole[a]		benzimidazole		benzotriazole	
	S_0	S_1	S_0	S_1	S_0	S_1
a	542(10)	480(35)	543(17)	477(10)	540(vs)	481(vs)
b	611(40)	540(42)	620(36)	566(45)	632(0)[b]	-
c	760(180)	718(175)	776(190)	729(175)	783(0)[b]	-
d	-	785(28)	-	-	-	795(vs)

a) data about indole are taken from [22]
b) Raman frequency taken from [15].

and d modes exhibit a ^1L_a character but that of b and c modes, a ^1L_b character. The ^1L_a or the ^1L_b character of bands is not reflected in their dispersed fluorescence spectra: the fluorescence spectra of indole [22] and benzimidazole following excitation into the a and b bands differ only with respect to the ground-state frequency. This can be explained if we assume that the strongest 1←1 band in fluorescence is induced by the same type transition as one finds for 0–0 band (^1L_b for indole and benzimidazole), although the relevant transition in absorption (1←0 band) may be either of ^1L_a or ^1L_b type.

In case of benzotriazole it is possible that one of the two different tautomers (Fig. 4.1) corresponds to the equilibrium configuration of the ground state, while the other tautomer, to that of the excited ^1L_a state. Briefly, proton transfer (tautomerization) accompanies the electronic transition. Proton transfer, dissociation by NH bond breaking and/or the crossing of the ^1L_a and ^1L_b potentials may be responsible for the rapid termination of the excitation spectrum of benzotriazole 1200 cm^{-1} above the ^1L_a origin. In case of benzimidazole the barrier is probably too high to see spectral manifestations of proton tunnelling.

References

[1] J.R.Platt, J.Chem. Phys. 19 (1951) 101
[2] H.-U.Schütt, H.Zimmermann, Ber. Buns. Phys. Chem. 67 (1963) 54
[3] M.R.Eftink, L.A.Selvidge, P.R.Callis, A.A.Rehms, J. Phys. Chem. 94 (1990) 3469
[4] E.H.Strickland, C.Billups, Biopolymers 12 (1989) 1973
[5] L.Philips, D.H.Levy, J. Chem. Phys. 85 (1986) 1327
[6] D.R.Demmer, G.W.Leach, E.A.Outhouse, E.A.Hager, S.C.Wallace, J. Phys. Chem. 94 (1990) 582
[7] D.M.Sammeth, S.Yan, L.H.Spangler, P.R.Callis, J. Phys. Chem. 94 (1990) 7340
[8] M.J.Tubergen, J.R.Cable, D.H.Levy, J. Chem. Phys. 92 (1990) 51
[9] S.Arnold, M.Sulkes, J. Phys. Chem. 96 (1992) 4768

[10] P.R.Callis, J. Chem. Phys. 95 (1991) 4230
[11] R.D.Gordon, R.F.Yang, Can J. Chem. 48 (1970) 1722
[12] E.Cané, A.Trombetti, B.Velino, W.Caminati, J. Mol. Spectry. 150 (1991) 222
[13] E.Cané, A.Trombetti, B.Velino, J. Mol. Spectry. 158 (1993) 399
[14] A.Suwaiyan, R.Zwarich, N.Baig, J. Raman. Spectry. 21 (1990) 243
[15] J.Rubim, I.G.R.Gutz, O.Sala, W.J.Orville-Thomas, J. Mol. Struct. 100 (1983) 571
[16] J.Elguero, C.Marzin, A.R.Katritzky, P.Linda, The Tautomerism of Heterocycles, Adv. Heterocycl. Chem., Suppl. 1, Acad. Press, New York, 1976
[17] A.Escande, J.L.Galigne, J.Lapasset, Acta Crystallogr. B30 (1974) 1490
[18] J.R.Cox, S.Woodcock, I.H.Hillier, M.A.Vincent, J. Phys. Chem. 94 (1990) 5499
[19] E.H.Jalviste, A.B.Treshchalov, Proc. Estonian Acad. Sci. Phys. Math. 40 (1991) 213
[20] T.L.Smithson, R.A.Shaw, H.Wieser, J. Chem. Phys. 81 (1984) 4281
[21] P.M.Felker, A.H.Zewail, J. Chem. Phys. 82 (1985) 2961
[22] Y.Nibu, H.Abe, N.Mikami, M.Ito, J. Phys. Chem. 87 (1983) 3898
[23] S.M.Beck, J.B.Hopkins, D.E.Powers, R.E.Smalley, J. Chem. Phys. 74 (1981) 43
[24] M.Fuji, T.Ebata, N.Mikami, M.Ito, Chem. Phys. 77 (1983) 191
[25] J.B.Coon, R.E.DeWames, C.M.Loyd, J. Mol. Spectry. 8 (1962) 285
[26] J.A.Syage, J.E.Pollard, J.Steadman, Chem. Phys. Lett. 161 (1989) 103
[27] М.Д.Франк-Каменецкий, А.В.Лукашин, УФН 116 (1975) 193
[28] H.Kupka, G.Olbrich, J. Chem. Phys. 82 (1985) 3975

Chapter 5

SUPERCRITICAL CO_2 AS A SOLVENT FOR SAMPLE INTRODUCTION INTO A SUPERSONIC JET FOR LIF SPECTROSCOPY

5.1 Introduction

It is well known that the supersonic jet technique permits the production of an ensemble of isolated molecules with very low rotational and vibrational temperatures desirable for spectroscopy. Laser-induced fluorescence (LIF) and resonance-enhanced two-photon ionization spectra (RE2PI) of jet-cooled large organic molecules consist of a relatively small number of narrow clearly-resolved vibronic bands.

Usually the jet of free, cold molecules of interest is formed by a simple heating of the sample in the atmosphere of a carrier gas (He or Ar) and a subsequent expanding of the mixture into vacuum. However, a large number of molecules (most of the biologically important molecules) are low-volatile and thermally instable: thermal decomposition of these molecules occurs at lower temperatures than the one providing enough vapour pressure for LIF spectroscopy.

Several sophisticated methods of introducing such molecules into a supersonic jet expanding into vacuum have been probed in order to avoid thermal decomposition:

- blowing the molecules out from hot surface of a metal cavity by the carrier gas pulses formed by a pulsed valve with subsequent free jet expansion (a sample film inside a cavity is prepared preceningly) [1],
- the same as the usual continuous jet technique, but instead of a pure sample a mixture of the sample powder with a specially chosen compound (uracil, diatomaceous earth) is used [2,3],
- pulsed laser desorption of the sample film prepared on a brass surface in a vacuum chamber and a subsequent cooling of the desorbed molecules penetrating into the expanding jet of the carrier gas [4],
- forming the jet by expansion of a supercritical fluid (CO_2, N_2O, Xe, freons, etc. in a supercritical phase) with dissolved

molecules of interest into vacuum [5].
The desorption method takes advantage of the shortness of the time interval during which molecules are exposed to high temperature for evaporation. In other methods (especially the supercritical fluid method) lowered (dangerless for decomposition) temperature is applied.

By definition the supercritical phase corresponds to pressures and temperatures exceeding their critical values. In the supercritical phase the difference between the gas and the liquid vanishes. Most often CO_2 is used as a supercritical fluid in practical applications, because CO_2 has easily achievable values of the critical temperature T_{cr} = 31.3 °C and the critical pressure P_{cr} = 72.9 atm.

Nowadays much attention is paid to a new chromatographic technique - supercritical fluid chromatography (SFC), where supercritical fluids are used as a mobile phase [6]. SFC separation can be applied also in case of the mixtures containing low-volatile and thermally instable compounds (taking advantage of relatively high solubility of these compounds in supercritical fluids), whose vapour pressure is not high enough for gas chromatography. Like other chromatographic methods SFC has a broad range of practical applications, for example environmental monitoring, analysis of foodstuffs and fuels, separation of drugs from mixtures etc. [7].

SCF chromatography with mass-selective detection has recently become an actual field of research [6,7]. Mass-selective detection without spectral selectivity is somewhat easier to realize, as no jet cooling is needed for that. The adding of the spectral dimension, which can be accomplished by equipping the SCF chromatograph with a supersonic jet interface for mass-selective RE2PI detection, may open new perspectives in chemical analysis. Therefore, in case of spectroscopic measurements, it is actual to investigate how the organic molecules dissolved in a supercritical fluid can be introduced into a jet expanding into vacuum. Although a number of results have been gained with mass-selective and/or RE2PI detection [6,7], we confine oneselves to LIF detection available to us. Some promising results in this field have already been achie-

ved: LIF spectra of jet-cooled perylene dissolved in CO_2 fluid [5] and LIF detection of jet-cooled chloroantracenes followed by separation with SCF chromatography [8].

This motivated us to probe the performance of the supercritical fluid method for well-studied test molecules quinizarin and phenol. The purpose was to apply this method to molecules (concretely to amino-acids tryptophan and tyrosine), whose spectra cannot be obtained by simple heating technique.

5.2 Experimental

The laser system based on ELI-5 excimer laser and VL-18 dye laser and the fluorescence registration system are described in Chapter 2 of this thesis.

For experiments with supercritical CO_2 a new jet system was assembled based on the design from Ref. [4] (see Fig. 5.1).

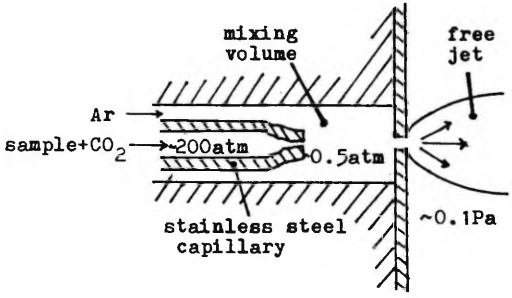

Figure 5.1: Schematic cross-section of the jet interface for LIF spectroscopy of jet-cooled molecules dissolved in supercritical CO_2.

Prior to measurements a HPP 5001 high-pressure piston pump for chromatograph was filled with CO_2 from a pressure vessel through a silica-gel dryer coloumn and a molecular-sieve filter coloumn. The gas collected into the piston pump was compressed until liquid CO_2 with the desirable pressure was formed (from 80 up to 500 atm). The pump was connected with a sample cell (extractor) mounted in an air-thermostate. The sample cell had previously been filled with the compound of interest. The

outlet of the cell is equipped with a porous metal filter to avoid the solid particles being carried forward. The temperature of the cell could be set from room temperature up to 100°C. If necessary, the supercritical conditions for CO_2 could be chosen for better dissolving of the sample.

The solution of the sample was directed through a 0.8 mm diameter (0.2 mm inner diameter) stainless steel capillary into a mixing volume (see Fig. 5.1), where CO_2 could be mixed with Ar in case better cooling in the jet was desired. The end of the capillary was squeezed in order to form a restrictor to be used for keeping high pressure in the system. The flow rate of CO_2 through the restrictor was adjusted by squeezing it with pliers until it was about 1 ml/min at 200 atm pressure. Higher flow rates and pressures resulted in a poor vacuum in the vacuum chamber because the evacuation capability of the vacuum pumps was exceeded. During the measurements the stationary pressure desired was ensured by selecting the proper speed of the pump piston. The piston speed is displayed on the scale of the selector switch directly in volume-flow-rate units (ml/min).

The length of the mixing volume (the displacement of the restrictor from the nickel foil with ≈200 μm orifice) was typically set to ≈2 mm. The pressure in the mixing volume (measured by a pressure gauge connected to the Ar inlet) was between 0.1 and 1 atm. In the vacuum chamber the jet containing cooled molecules of interest intersected the laser beam. The stainless-steel capillary from the sample chamber to the restrictor was heated up to 100°C with 2-3 A current directed through it and the temperature in the mixing volume was kept at 100-150°C by heating the jet assembly with a wire heater. Additional heating of the jet assembly was necessary to avoid the clustering of CO_2, which eventually lead to the freezing (by Joule-Thompson effect) and the clogging of the restrictor.

5.3 Results and discussion

At first test experiments with phenol and quinizarin were carried out with the aim to optimize the experimental condi-

tions (temperatures and pressures in the sample cell and the mixing volume and the flow rate of Ar) for LIF measurements.

The 0-0 band rotational contour of phenol excitation spectrum is presented in Fig. 5.2. The adding of Ar gas into the mixing volume yielded a contour compressed about two times (T_{rot}=9 K) as compared with the one obtained by using pure CO_2 as a coolant (T_{rot}=35 K). The rotational temperatures were estimated from the distance between the maxima of P and R branches as described in Chapter 2. For quinizarin the same effect was observed: the adding of Ar lowered the rotational temperature. Worsened cooling with pure CO_2 can be explained by the release (storing into the translational-rotational bath) of the thermal energy from CO_2 vibrational degrees of freedom via vibrational relaxation of CO_2 during expansion into vacuum.

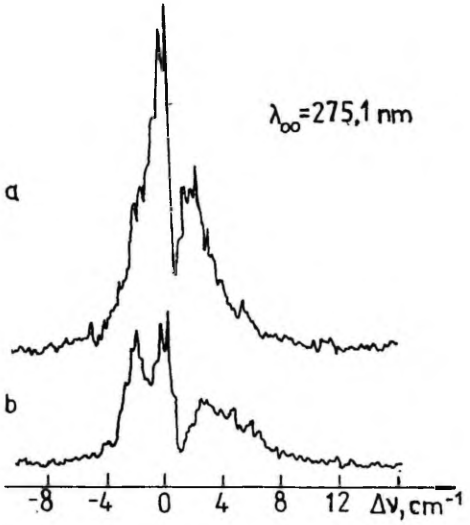

Figure 5.2: Rotational contour of phenol 0-0 band at different measuring conditions: a) without Ar (p=24 kPa in the mixing volume); b) with Ar (p=44 kPa: 24 kPa of CO_2 and 20 kPa of Ar). Conditions in the sample cell: P=200 atm and T=40°C.

Fluorescence excitation spectrum of phenol is presented in Fig. 5.3. Towards the red from the most intense 0-0 band at

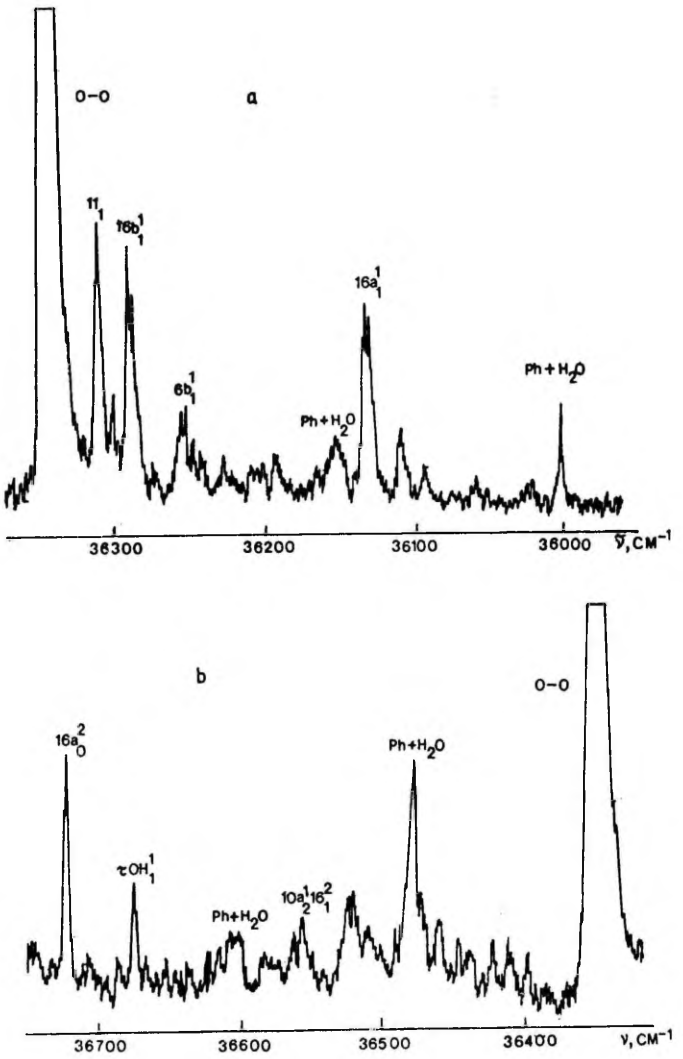

Figure 5.3: Fluorescence excitation spectrum of phenol: a) region to the red from the 0-0 band; b) region to the blue from the 0-0 band (P=200 atm, T=40°C, p=44 kPa)

36349 cm^{-1} (275.1 nm) there are weak bands with the intensities being some percent of 0-0 intensity. A majority of these weak vibronic bands are assigned to hot bands by comparing our spectrum with the phenol vapour absorption spectrum presented in Refs. [9,10]. Most of the hot bands represent 1-1 transitions of the modes of the benzene frame. The intensities of hot bands were quite insensitive to Ar addition. The vibrational temperature was estimated to be on the average 150 K, based on experimental band intensities and ground state vibrational frequencies from Refs. [9,10].

Besides hot bands some bands belonging to Van-der-Waals complexes of phenol with 1 up to 3 water molecules were identified. Among these the strongest (the 0-0 band of the phenol-H_2O complex) is shifted 353 cm^{-1} to the red from the 0-0 band of bare phenol [11]. Some bands red-shifted from vibronic bands of bare phenol were also assigned to phenol-$(H_2O)_n$ complexes (they were located to the blue from 0-0 band of phenol). Among these the strongest band had 353 cm^{-1} red shift from 6a vibronic band. The weaker bands assigned to phenol-water complexes with two or more water molecules had very poor reproducibility. The water additive may come from phenol sample itself (no attempts were made to purify and dry it) or from CO_2 despite drying it with silica gel water absorber.

Both quinizarin and phenol are thermally stable molecules and their jet spectra can easily be obtained by the standard technique. However, we showed that for the supercritical technique the heating of the sample cell up to 40°C and the heating of the capillary up to 100°C is enough to get a normal signal. In case of the ordinary continuous jet technique the quinizarin powder should be heated up to 140°C to get the vapour pressure necessary for LIF measurements. The lowering of the temperature in the sample cell below 31.5°C (by using liquid CO_2 instead of supercritical) did not change the signal noticeably. All the spectra obtained were still very noisy and poorly reproducible, probably because of a fluctuating gas flow out of the restrictor. A serious complication that often occured was the clogging of the restrictor.

Initially we used a 50 μm inner-diameter quartz capillary

with a restrictor formed by the stretching of the capillary in a gas flame and the subsequent cutting. A visual observation of the clogged restrictor by microscope showed red crystals of quinizarin recrystallized from CO_2 solution in the narrowing end of the capillary. The recrystallization there is greatly favoured by lower temperature and pressure. The restrictor (squeezed tip) of a heatable stainless steel capillary appeared to be more immune against clogging (probably because of its shortness and higher temperature) and it was restorable in case the clogging occurred. Therefore, afterwards we used only the stainless steel capillary.

We also tried to get the excitation spectra of amino acids tyrosine and tryptophan (their origins lye close to 281 nm and 287 nm, respectively). These molecules have a very low vapour pressure because of a large permanent dipole moment induced by amino and carboxyl groups. Experiments aimed at getting their jet spectra by an ordinary method failed: a black viscous compound was formed in the cases when tyrosine or tryptophan was kept at $\approx 300^{\circ}C$ for a long time (about an hour). Nevertheless, nice spectra of tryptohan were obtained by heating one-to-one mixture of tryptophan and uracil powder at temperature $210^{\circ}C$ and a subsequent cooling in a continuous Ar jet [2]. Despite our efforts we did not get any signal by using supercritical technique. It is possible that tryptophan and tyrosine have very low solubility in supercritical CO_2, as the clogging of the restrictor occurred rarely compared to experiments with quinizarin and phenol. Moreover, almost all the tyrosine powder inserted into the sample cell remained there after several hours of measurements, while in an analogous case quinizarin and phenol were completely lost. The neglible solubility of tyrosine and tryptophan in CO_2 and N_2O supercritical fluids was stated also in Ref. [12]. We tried to increase the solubility by adding a polar solvent (methanol) to CO_2, nevertheless, LIF signal was not achieved.

To investigate the stability of the gas flow (which determines the quality of the spectra) the flow out of the restrictor (into ambient air) was visualized by illuminating it from one side. A conically expanding fan of CO_2 clusters was

observed with slightly fluctuating density and shape. The solubility of samples was qualitatively examined by directing the flow from the restrictor to a glass plate. In case of quinizarin a red spot was formed by ≈10 s, but for a tyrosine sample only a water drop condensed from the ambient air was formed on the glass plate. However, after a long-time exposure (10 min) and the drying of the plate a thin tyrosine film was left.

A detailed experimental and theoretical study of the performance of capillary restrictors, where the conditions leading to the onset of clustering were elucidated, is presented in Ref. [13]. In principle, condensation should not occur if the initial pressure and temperature are such that during the adiabatic expansion CO_2 remains gaseous. For example, more than 140°C is needed at ≈200 atm pressure to avoid condensation according to CO_2 phase diagram, hence additional preexpansion (in the mixing volume in our construction) is not necessary. However, in case of the gas coming out of the restrictor was directly expanded into vacuum, the formation of macroscopic CO_2 clusters (droplets) made LIF measurements impossible because of the scattering of the laser light. Maybe it is easier to keep the restrictor hot by using a construction with a mixing volume, because otherwise, the bare restrictor ending in the vacuum chamber is quickly cooled down by the Joule-Thompson effect, resulting in an extensive clustering. The collisional dissociation of CO_2 clusters may also play an important role during the preexpansion in the mixing volume.

Our experience shows that the introduction of a sample dissolved in a supercritical fluid into a free jet for LIF detection is feasible, however, because of technical complications (the clogging of the restrictor, poor quality of the spectra), very tedious and troublesome. Nevertheless, this method may be suite well for some other fluorescing biomolecules.

References

[1] T.R.Rizzo, Y.D.Park, L.A.Peteanu, D.H.Levy, J. Chem. Phys.

84 (1986) 2534

[2] L.A.Philips, S.P.Webb, S.J.Martinez III, G.R.Fleming, D.H.Levy, J. Am. Chem. Soc. 110 (1988) 1352

[3] J.Sipior, M.Sulkes, R.Auerbach, M.Boivineau, J. Phys. Chem. 91 (1987) 2016

[4] J.R.Cable, M.J.Tubergen, D.H.Levy, J. Am. Chem. Soc. 110 (1988) 7349

[5] H.Fukuoka, T. Imasaka, N.Ishibashi, Anal. Chem. 58 (1986) 375

[6] Supercritical Fluid Chromatography. Ed. by R.M.Smith. The Royal Society of Chemistry, 1988 (Сверхкритическая флюидная хроматография, Под ред. Р.Смита, Мир, 1991)

[7] Abstracts of the Pittsburgh Conference and Exposition on Analytical Chemistry and Applied Spectroscopy, 1988

[8] T.Imasaka, N.Yamaga, N.Ishibashi, Anal. Chem. 59 (1987) 419

[9] H.D.Bist, C.D.Brand, D.R.Williams, J. Mol. Spectry. 21 (1966) 76

[10] H.D.Bist, C.D.Brand, D.R.Williams, J. Mol. Spectry. 24 (1967) 413

[11] H.Abe, N.Mikami, M.Ito, J. Phys. Chem. 86 (1982) 1768

[12] L.Li, D.M.Lubman, Rev. Sci. Instrum. 59 (1988) 557

[13] R.D.Smith, J.L.Fulton, R.C.Petersen, A.J.Kopriva, B.W. Wright, Anal. Chem. 58 (1986) 2057

MAIN RESULTS

1. Saturation curves (fluorescence intensity as a function of excitation intensity) of jet-cooled quinizarin excited into the 0-0 band of $S_1 \leftarrow S_0$ transition (at 19917 cm^{-1}) have been measured by using a pulsed dye laser. The saturation curve measured under 0.045 cm^{-1} FWHM excitation exhibits the transition from linear dependence to sqare-root dependence at the (saturation) intensity of 150 W/cm^2. The observed square root dependence at high excitation intensities is explained in terms of inhomogeneously broadened (thanks to the rotational structure) two-level system. The influence of time-dependent and laser mode-structure effects on the saturation curve are discussed and estimated.

2. Rotational contour of the 0-0 band of quinizarin has been recorded at various excitation intensities. The broadening of the Q branch from 0.045 cm^{-1} (at 100 W/cm^2) up to 0.4 cm^{-1} (at 10^6 W/cm^2) is interpreted as a power broadening. Out-of-plane symmetry is assigned to all non-totally symmetric vibrations of S_1, appearing in the excitation spectrum up to 486 cm^{-1} mode, based on the rotational contour analysis of respective vibronic bands.

3. Transition strength characteristics of quinizarin $S_1 \leftarrow S_0$ origin band have been determined by using the measured saturation intensity and the known lifetime of S_1 0-level (3.8 ns). The transition dipole moment of 0.74 D and the oscillator strength of 0.005 have been obtained. The fluorescence quantum yield has been estimated to be 2.5%.

4. The polarization degree of the undispersed laser induced fluorescence following excitation into the 0-0 band of jet-cooled quinizarin has been measured as a function of excitation frequency and intensity. Excitation into the Q branch results in a more polarized fluorescence (the maximum value of the polarization degree was ≈17%) than the excitation into the P or R branch (maximum degree was ≈9%). The polarization degree decreases along with the rise of the intensity of the excitation pulse and remaines constant (of ≈2%) if the ecxitation

intensity exceeds $6*10^3$ W/cm^2 independent of the branch being excited.

5. The results of polarization saturation experiments are compared with theoretical predictions. The quinizarin jet is modelled with a thermally populated ensemble of freely rotating symmetric tops, taking into account saturation in case of inhomogeneous broadening. A simple interpretation of the difference of the fluorescence anisotropy following excitation into the Q branch and P or R brances is presented.

6. Laser-induced S_1-S_0 fluorescence excitation and dispersed fluorescence spectra of jet-cooled benzimidazole and benzotiazole molecules have been measured for the first time. The first excited singlet state is assigned to ^1L_b for benzimidazole (origin at 36032 cm^{-1}) and to ^1L_a for benzotriazole (origin at 34927 cm^{-1}).

7. The correspondence between the vibrational modes of S_1 and S_0 states has been established for benzimidazole on the ground of dispersed fluorescence spectra following the excitation into the respective vibronic bands. For the modes with frequencies below 800 cm^{-1} one-to-one correspondence has been found, but for higher-frequency vibrations mode mixing has been observed. A Franck-Condon analysis of the breathing mode (729 cm^{-1} in S_1 and 776 cm^{-1} in S_0) yielded a distortion parameter of 0.7.

8. The absence of fluorescence for benzotriazole excited higher than 1300 cm^{-1} above its S_1 origin is explained by a rapid nonradiative decay. A vibrational analysis revealed that the progressions of several in-plane modes (540, 1153, 1242, 1405, and 1447 cm^{-1}) cover about 8000 cm^{-1} of the dispersed fluorescence spectrum following the excitation into the origin of the S_1 (^1L_a) state of benzotriazole. The intensity maximum of this spectrum has been found to lie in the region where three quanta of 1153, 1242, 1405, and 1447 cm^{-1} modes combine.

9. A comparative analysis of the excitation and S_1 0-level fluorescence spectra of benzimidazole, benzotriazole, and indole has permitted the assignment of ^1L_a and ^1L_b types to several low-frequency (< 800 cm^{-1}) modes common for these molecules.

MÕNEDE JOAS JAHUTATUD ORGAANILISTE MOLEKULIDE LASERSPEKTROSKOOPIA

PÕHITULEMUSED

1. On saadud küllastuskõverad (fluorestsentsi intensiivsuse sõltuvus ergastuse intensiivsusest) joas jahutatud kinisariini molekuli $S_1 \leftarrow S_0$ ülemineku 0-0 joone (19917 cm^{-1}) jaoks. Küllastuskõvera korral, mis on mõõdetud 0.045 cm^{-1} spekraallaiusega ergastusel impulss-värvlaseriga, toimus üleminek lineaarselt sõltuvuselt ruutjuursõltuvusele (küllastus) intensiivsusel 150 W/cm^2. Ruutjuursõltuvust suurtel ergastusintensiivsustel on seletatud kui küllastusefekti mittehomogeenselt laienenud (tänu pöörlemisstrtruktuurile) kahenivoolise süsteemi korral. On hinnatud ajast sõltuvate ja laseri moodstruktuuri effektide mõju küllastuskõverale.
2. Kinisariini 0-0 joone pöörlemiskontuur on registreeritud erinevate ergastusintensiivsuste korral. Pöörlemiskontuuri Q haru laienemist 0.045 cm^{-1}'st 100 W/cm^2 intensiivsusega ergastusel kuni 0.4 cm^{-1}'ni 10^6 W/cm^2 korral on tõlgendatud küllastus-laienemise avaldumisena. Vibroonjoonte pöörlemiskontuuride analüüsi tulemusena on kindlaks tehtud, et kõik ergastusspektris esinevad S_1 seisundi mittetäisstmmeetrilised võnkumised kuni 486 cm^{-1} võnkumiseni omavad sümmeetriat, mille korral aatomite nihked or risti molekuli tasandiga.
3. Mõõdetud küllastusintensiivsuse ja teadaoleva S_1 seisundi põhitaseme eluea (3.8 ns) põhjal on määratud kinisariini 0-0 joone üleminekutõenäosust iseloomustavad parameetrid: ülemineku diipolmoment (0.74 D) ja ostsillaatori jõud (0.005). Fluorestsentsi kvantsaagis on hinnatud ≈2.5%'le.
4. On uuritud joas jahutatud kinisariini spektraalselt lahutamata fluorestsentsi polarisatsiooni sõltuvust ergastuse intensiivsusest ja sagedusest. 0-0 joone pöörlemiskontuuri Q harru ergastamine andis rohkem polariseeritud fluorestsentsi (maksimaalne polarisatsiooni aste 17%) kui P või R harru ergastamine (maksimaalne aste 9%). Ergastusintensiivsuse kasvul muutus fluorestsents vähem polariseerituks. Kui ergastuse intensiivsus ületas $6*10^3$ W/cm^{-1} jäi fluorestsentsi polarisa-

intensity exceeds $6*10^3$ W/cm^2 independent of the branch being excited.

5. The results of polarization saturation experiments are compared with theoretical predictions. The quinizarin jet is modelled with a thermally populated ensemble of freely rotating symmetric tops, taking into account saturation in case of inhomogeneous broadening. A simple interpretation of the difference of the fluorescence anisotropy following excitation into the Q branch and P or R brances is presented.

6. Laser-induced S_1-S_0 fluorescence excitation and dispersed fluorescence spectra of jet-cooled benzimidazole and benzotiazole molecules have been measured for the first time. The first excited singlet state is assigned to ^1L_b for benzimidazole (origin at 36032 cm^{-1}) and to ^1L_a for benzotriazole (origin at 34927 cm^{-1}).

7. The correspondence between the vibrational modes of S_1 and S_0 states has been established for benzimidazole on the ground of dispersed fluorescence spectra following the excitation into the respective vibronic bands. For the modes with frequencies below 800 cm^{-1} one-to-one correspondence has been found, but for higher-frequency vibrations mode mixing has been observed. A Franck-Condon analysis of the breathing mode (729 cm^{-1} in S_1 and 776 cm^{-1} in S_0) yielded a distortion parameter of 0.7.

8. The absence of fluorescence for benzotriazole excited higher than 1300 cm^{-1} above its S_1 origin is explained by a rapid nonradiative decay. A vibrational analysis revealed that the progressions of several in-plane modes (540, 1153, 1242, 1405, and 1447 cm^{-1}) cover about 8000 cm^{-1} of the dispersed fluorescence spectrum following the excitation into the origin of the S_1 (^1L_a) state of benzotriazole. The intensity maximum of this spectrum has been found to lie in the region where three quanta of 1153, 1242, 1405, and 1447 cm^{-1} modes combine.

9. A comparative analysis of the excitation and S_1 0-level fluorescence spectra of benzimidazole, benzotriazole, and indole has permitted the assignment of ^1L_a and ^1L_b types to several low-frequency (< 800 cm^{-1}) modes common for these molecules.

ACKNOWLEDGEMENTS

I am grateful to all of my present and previous colleagues from the Laboratory of Laser Technique and to all those whose contribution (constructing and making new parts for the apparatus, providing materials, gases, chemicals and computer software, giving good advice, etc.) made possible the realization of the investigations reflected in this thesis. Special thanks I devote to my long-time supervisor Aleksei Treshchalov for his kind support he provided at all the stages of the work including the attentive revision of the thesis. I am indebted also to Prof. Jörg Reuss from Nijmegen, who helped me in publishing one of my articles in Chemical Physics and to Evi Vaik for proof-reading of the English manuscript.

CONFERENCES

1. Первая республиканская школа-семинар "Методы лазерной биофизики и их применение в медицине", Тарту 1988
2. Всесоюзный семинар "Спектроскопия свободных сложных молекул", Минск 1988
3. Второй всесоюзный семинар "Лазерная биофизика и новые применения лазеров в медицине", Кяэрику 1989
4. Семинар по лазерной спектроскопии, Лохусалу 1990
5. Fourth European Conference on Atomic and Molecular Physics, Riga 1992.
6. Annual Conference of the Departments of Molecular Spectroscopy and Physical Chemistry of the Dutch Foundation for Chemical Research (SON), Lunteren 1993
7. 4th Nordic-Baltic Workshop on Photochemisty, Tartu 1993

PUBLICATIONS

1. В. Т. Михкельсоо, А. Б. Трещалов, В. Э. Пеэт, Э. Х. Ялвисте, А. А. Белоконь, Б. И. Брайнин, К. М. Хритов, Образование эксимерных молекул XeCl при смешении газовых потоков, возбужденных непрерывным разрядом, Квантовая Электроника 14, 7 (1987) 1404-1406 (not reflected in this thesis)
2. В. Т. Михкельсоо, А. Б. Трещалов, В. Э. Пеэт, Э. Х. Ялвисте, Е. В. Сливинский, А. А. Белоконь, Б. И. Брайнин, К. М. Хритов, Непрерывный источник эксимерной флуоресценции, основанный на смешении возбужденных газовых потоков, Труды ИФ АН ЭССР 60 (1987) 7-14 (not reflected in this thesis)
3. А. Б. Трещалов, С. А. Царенко, Э. Х. Ялвисте, В. Т. Михкельсоо, Э. К. Сеппет, Н. О. Пеэт, Лазерная спектроскопия органических молекул, охлажденных в сверхзвуковой струе, в сб. Методы лазерной биофизики и их применение в медицине, материалы докладов, Тарту 1988, 126-137 (Chapter 1)
4. Э. Х. Ялвисте, А. Б. Трещалов, Влияние насыщения на колебательно-вращательные контуры в спектре возбуждения хинизарина, охлажденного в сверхзвуковой струе, ЖПС. 53, 3 (1990) 449-456 (Chapter 2)
5. Э. Х. Ялвисте, А. Б. Трещалов, Проявление эффекта насыщения в поляризации флуоресценции охлажденных в сверхзвуковой струе молекул хинизарина, ЖПС. 53, 4 (1990) 567-572 (Chapter 3)
6. А. Б. Трещалов, С. А. Царенко, Э. Х. Ялвисте, В. Т. Михкельсоо, Н. О. Пеэт, Спектроскопия органических молекул, охлажденных в сверхзвуковой струе, с использованием сверхкритического CO_2 в качестве носителя, в сб. Лазерная биофизика и новые применения лазеров в медицине, материалы докладов, Тарту 1990, 274-281 (Chapter 5)
7. E. H. Jalviste, A. B. Treshchalov, Spectroscopic study of jet-cooled benzotriazole, Proc. Estonian Acad. Sci. Phys. Math. 40, 3 (1991) 213-220 (Chapter 4)
8. Erko Jalviste, Aleksei Treshchalov, Spectroscopy of jet-cooled benzimidazole and benzotriazole, Chem. Phys. 172, 2-3 (1993) 325-338 (Chapter 4)